Local Anodic Modification of Si substrates Covered with a Self-Assembled Monolayer by Scanning Probe Microscopy

Jiwon Han

March, 2009

Local Anodic Modification of Si substrates Covered with a Self-Assembled Monolayer by Scanning Probe Microscopy

（走査型プローブ顕微鏡による有機単分子膜被覆シリコン基板の局所的陽極酸化）

Jiwon Han

March, 2009

Department of Materials Science and Engineering,
Kyoto University

Dissertation submitted in partial fulfillment of the requirements for the degree of DOCTOR OF ENGINEERING

Contents

1. Introduction

1.1. Motivation

The miniaturization of electronic devices is the pursuing purpose and challenge of the electronic industries. The transistor and the microprocessor, that is, the most important invention in modern science history, were born in 1947 and in 1971, respectively. These inventions made the industries of the world develop dramatically, and those made it possible for the people to use the smaller electronic devices such as a notebook computer, a cellular phone, a digital audio play (commonly referred to as MP3 player), etc. Intel founders, Moore and Gordon, expected a semiconductor integration to increase two times each one and a half to two years. Moore′s law are describing semiconductor situation well. In the 21th century, the Intel published Pentium 4 consisting of 4200 million transistors. To improve the integration, they must have reduced a circuit line width to 0.13 micron. In 2008, dynamic random access memory devices have already reached a limit of 57 nm half-pitch. In 2015, the memory needs to be fabricated below a 25 nm half-pitch.

One of the important technologies related to the miniaturization of these devices is focused on how small structures can be fabricated to a desired point and how to observe such structures. The core of these technological requirements will be fulfilled by scanning probe microscopy (SPM). Scanning tunneling microscopy (STM)[1)] and atomic force microscopy (AFM),[2)] etc, which are generally named as SPM, can obtain high resolution surface images of materials and also fabricate nano-scale patterns on semiconductor and metal substrates using a fine SPM tip.[3-5)]

There are several methods for fabricating nanoscale patterns on a bulk surface using SPM. Direct scratch lithography,[6)] dip-pen lithography,[7,8)] and SPM-based anodization[9,10)] are well known for their capability to make nanosize structures.

Among these methods, SPM anodization can fabricate extremely small oxide on a substrate through local electrochemical reactions in the adsorbed water meniscus existing between the SPM tip and the surface. This method can be operated in air and can be applied to a wide variety of important electronic materials including Si for fine structuring. SPM anodization itself can fabricate nanoscale oxide patterns on Si surfaces. However, it has problems of contamination and oxidation of Si surfaces due to the patterning process performed in air. These problems will be solved by covering the Si surface with self-assembled monolayer (SAM).

The SAM is a molecular assembly, which is formed spontaneously by the immersion of an appropriate substrate in a solution of precursor molecules.[11] In other words, using SAM properties, which are well voluntarily parallel to each other, the uniform film with molecule level of about 1-2 nm thick is obtained. The kind of SAMs on Si can be roughly classified by the existence of an oxide layer between the SAM and the Si surface. One is organosilane SAMs and the other is directly attached SAMs. Here, the SAM directly attached to Si will be good films for SPM anodization, because of the preservation of Si atomic surface flatness without oxidation about for two months or more. It has been known that the flatness is required to obtain an atomic or molecular level manipulation. Because, fabricating processes based on electrochemical reaction depend on the state of surfaces, such as atomic vacancy, impurity atom, disorderly atomic arrangement, and surface step etc.[12] Such a SAM can be used for an oxidation barrier and an etching mask due to high chemical durability, which come from intensive chemical bond strength.

Features fabricated by SPM anodization are needed to be evaluated. Not only their structures but also physical properties have to be elucidated. Among several developed SPM techniques, Kelvin-probe force microscopy (KFM) for measuring

surface potential[13,14] and scanning capacitance microscopy (SCM) for differential capacitance[15,16] are promising methods for characterization of electrical properties. These also attract attention to charge writing and erasing onto dielectric materials by applying a bias voltage.[17-21]

Nanopatterns fabricated by SPM anodization are applicable to nano templates for the arrangement of minute objects as well. To apply an electric, optical, bio, and sensor devices in practice, nano structuring by nano-particles has attracted attention. Fabricating a nanostructure on bulk surfaces has been performed by several groups,[22,23] of which some reported its three- and two-dimensional array. If thinking about the application, one-dimensional array is of particular importance. But, few results are reported, because the precise control of nano-particles is difficult. Consequently, by using SPM anodization and properties of the terminal functional group of a SAM attached to bulk surfaces, a selective immobilization and an array research will be one of the challenge in nanotechnology.

1.2. Objectives

The objectives of this thesis are to optimize a nanostructuring technology based on SPM anodization on the direct-attach SAM/Si samples, and to evaluate electrical properties of the structured regions of SAM-covered Si substrates. Furthermore, we are aiming to concentrate one-dimensional nano-particle structuring for the application of the nano-structured surface.

To state clearly,

I. When SPM anodization is conducted, it is known that the meniscus at the contact point between the tip and the substrate is important factor in size of a fabricated line. Surface hydrophilicity, relative humidity, and tip materials are,

therefore, investigated for minute fabricating, because those affect the meniscus size.

II. Electrical properties on the voltage-biased region are investigated by KFM and SCM.

III. One-dimensional array of Au nanoparticles is performed using SPM anodization method and properties of SAM terminal group.

1.3. Scanning probe anodization (SPA)

SPM is outstanding invention in surface manipulation field below atomic or molecular level.[24-27] So far, although several manipulation principles are being supported and newly fabricated structures are being developed, the way through chemical reactions is considered to be important subjects. For examples, electron beam chemical vapor deposition and electron beam resist layer[28,29] were exposed by electrons emitted from a SPM probe tip. Polymerization of absorbed molecules[30] and regional hydrogenation of Si surface[31] were performed in nanoscale range by applying a bias voltage between a tip and a sample. It was further chemical reaction method that a SPM tip was acted as catalyst. A sample surface was locally hydrogenated by a SPM tip coated with Platinum and Palladium group metal, and surface chemical modification was done by a tip coated with the organic molecules of an enzyme and an organic sulfone acid.[32-36] Among methods of SPM-based chemical reactions, a general way to locally manipulate surfaces is electrochemical reactions into an absorbed water meniscus between a tip and a sample surface.[5,6] This method can be usually done in air rather than in a special environment like vacuum or solution, and applied to the fine fabrication process of important electronic materials such as Si.

In 1990, it was first reported that an oxidizing reaction occurred onto a semiconductor surface underneath a STM tip. Dagata et al. showed that such a

chemical change process performed under positive-biased tip on hydrogen-terminated Si surface in air could be applicable to a wide range of nanoscale structure fabrication.[3] The process was explained as follows. Hydrogen attached to Si atoms of the outer surface was desorpted by an applied electric field between the tip and the H-Si sample, and oxidation reactions were prompted. After STM oxidation process on Si substrates was reported, many similar researches were done. For metal, Thundat et al. showed a new oxidation process on Ta surface in air or alkaline solution by STM, which was performed under a sample being biased positively, although the process done by Dagata et al. was under a positive biased tip against the sample.[37] MacCarley et al. investigated why an etching occurred on graphite surfaces, when the STM was scanned. They concluded that an anodic reaction on the sample, which is a half-electrochemical reaction made the etching of graphite, because Faradaic current flowed through the water column between the tip and sample.[9]

Consider the basic principle of electrochemistry. It can be thought that an anode oxidation in a positive electrode is general rather than a cathode oxidation in a negative electrode, and that nanoscale fabrication is possible to other several materials as well as graphite. Indeed, Sugimura et al. fabricated nanoscale patterns on Ti metal surface using STM,[5] showing an anode oxidation reaction depended on adsorbed layer.[10] Many reports on the SPA of several materials are showed in table 1.[38-49]

If an SPM tip is approaching to the sample surface in air or wet environment, adsorbed layers of both the tip and the sample surface contact each other, and surface tension forms a fine column, namely meniscus, at the contact point between the tip and surface.[50,51] Figure 1 shows the water meniscus worked as a minute

Table 1. Materials patternable in SPM anodization

Materials		References
Semiconductors	Si, Si-H, SiO_2/Si	3, 4, 38, 39, 40
	SiGe	41
	GaAs	4
Metals	Al	42
	Co	43
	Cr	44
	Mo	45
	Ta	46
	Ti	5, 10
	Ni	43
Carbon	Graphite	9
	Amorphous carbon	47
	Diamond	41
Organic materials	Self-assembled monolayers	48
	Langmuir-Blodgett films	49

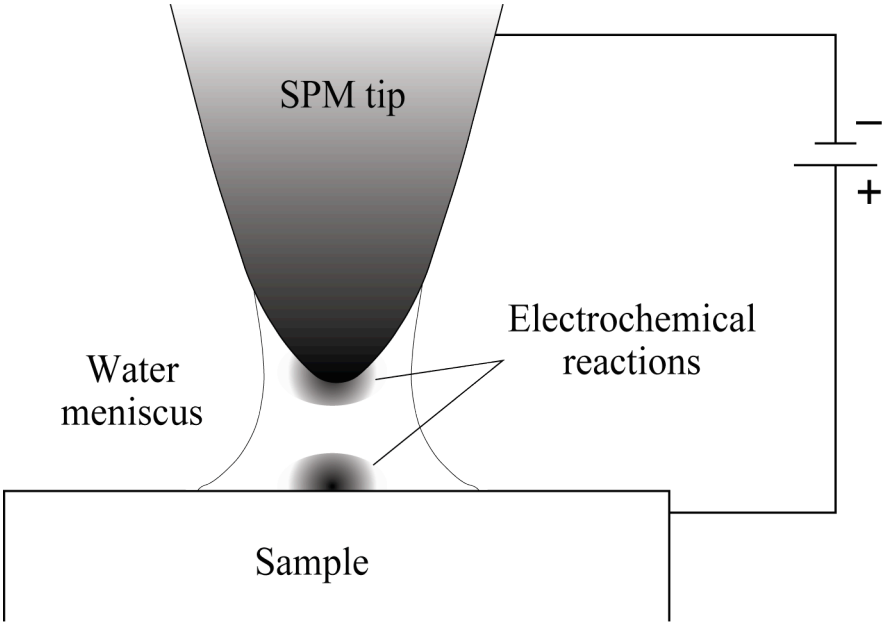

Tip (cathode) reaction:

$2nH_2O + 2ne^- \rightarrow nH_2 + 2nOH^-$

Sample (anode) reaction:

$M + nH_2O \rightarrow MO_n + 2nH^+ + 2ne^-$

Fig. 1. Schematic illustration of scanning probe anodization

electrochemical cell, in which anode oxidation, namely anodization, occurs. The electrochemical reaction has been suggested as follows. The net electrochemical reaction of the interfaces of water-oxide and oxide-sample substrate is shown in (1-1).

Sample (anode) reaction: $M + nH_2O \rightarrow MO_n + 2nH^+ + 2ne^-$ (1-1)

Hydrogen generation most certainly occurs at the tip electrode as the counter electrochemical reaction shown in (1-2).

Tip (cathode) reaction: $2nH_2O + 2ne^- \rightarrow nH_2 + 2nOH^-$ (1-2)

Although the water meniscus itself and the origin of electrochemical reaction have not been sufficiently considered yet, several research groups have recognized advantages of local anode oxidation using SPM, that is scanning probe anodization (SPA).[38,39)]

Local oxidized growth using SPM is sometimes called field-enhanced oxidation. The more intensive potential gradient would be thought to occur at the interface of the SPM tip and the sample surface than usual, resulting in the acceleration of chemical reactions. However, the magnitude of the potential gradient underneath the tip is about 1 V/nm. This value is not so large, when compared with the potential gradient of the inside of the oxidized film during anodization or of the electric double layer at electrode surface.

1.4. Self-assembled monolayer (SAM)

The SAM is formed through self-assembling, as can be known from the word itself. Proper precursor molecules will be spontaneously attached to a bulk surface, if the attachment can contribute to stabilization of both surface atoms of substrates and precursor molecules through chemical reaction. It has been known that the arrangement and packing of the molecules on the substrate comes from inter-molecule interactions, such as van der Waals.[11)] Figure 2 shows the simple SAM preparing

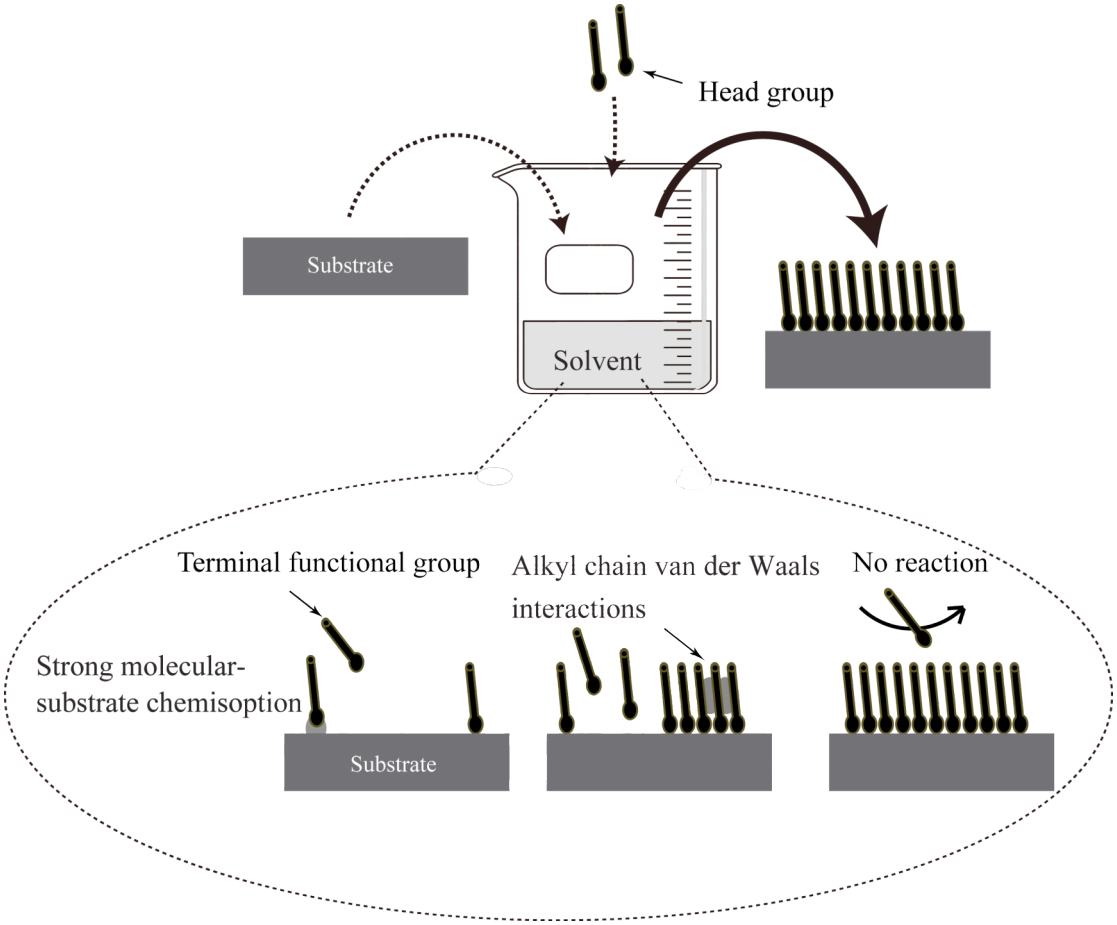

Fig. 2. Preparation process for SAM

Table 2. Pairs of precursors and substrates.

Materials	References
Organosulfurs alkylthiol: R–SH dialkyldisulfide: RS–SR' thioisocyanide: R–SCN etc.	Metals/compound semiconductors (Au, Ag, Cu, Pt, Pd, Hg, Fe, GaAs, InP, etc.)
Fatty acid R–COOH	Oxide (Al_2O_3, AgO, CuO, etc.)
Phosphonic acid $R–PO_3H_2$	Oxide (ZrO_2, TiO_2, Al_2O_3, Ta_2O_5, etc.)
Organosilanes: $R–SiX_3$ (X = Cl, OCH_3, OC_2H_5)	Oxide (glass, mica, SiO_2, SnO_2, GeO_2, ZrO_2, TiO_2, Al_2O_3, ITO, PZT, etc.)
Unsaturated hydrocarbons alkene, alkyne: R–CH = CH_2, R–C≡H Alchols, Aldehydes R–OH, R–CHO	Silicon [hydrogen-terminated Si: Si–H, (halogen-terminated Si: Si–X (X = Cl, Br, I)]

process. The well-ordered SAM was formed on a substrate immersed in the solution of precursor molecules. After the SAM is formed on a substrate, no more reaction occurs each other. It is a self-stop process. The film thickness can be, therefore, controlled very easily, depending on the length of precursor molecules. There are several kinds of self-assembling method, which forms the monolayers. For example, pairs of precursors and substrates were summarized in Table 2. These SAMs formed to a substrate have a possibility of application as detectors for bio and chemical sensors due to selectively adsorbing properties of their terminal functional group,[52-54] as barrier films for electronic devices,[55,56] and as resist films for nano-patterning process.[48,57,58]

1.4.1. SAM formation on Si substrates through the silane coupling reaction

The opening of organosilane SAMs formed on a Si substrate was reported by Sagiv et al.[59,60] Organosilane SAMs which are combined with Si substrates are chemically stable and mechanically strong. If the mechanism of SAM formation is explained, alcohoxy groups (for our experiment) of organosilane molecules are converted to silanol groups by hydrolysis, as shown in Fig. 3. The silanol groups react with hydroxyl groups of a Si substrate and with neighboring other silanol groups through dehydration reaction, so that the molecules were attached to the substrate. This reaction is called silane coupling. The chain reaction through hydrolysis and dehydration progresses, resulting in forming complicated siloxane two-dimensional networks. Such silane networks almost cover surfaces of the substrate, so reaction sites existing on the surface is screened and hidden.

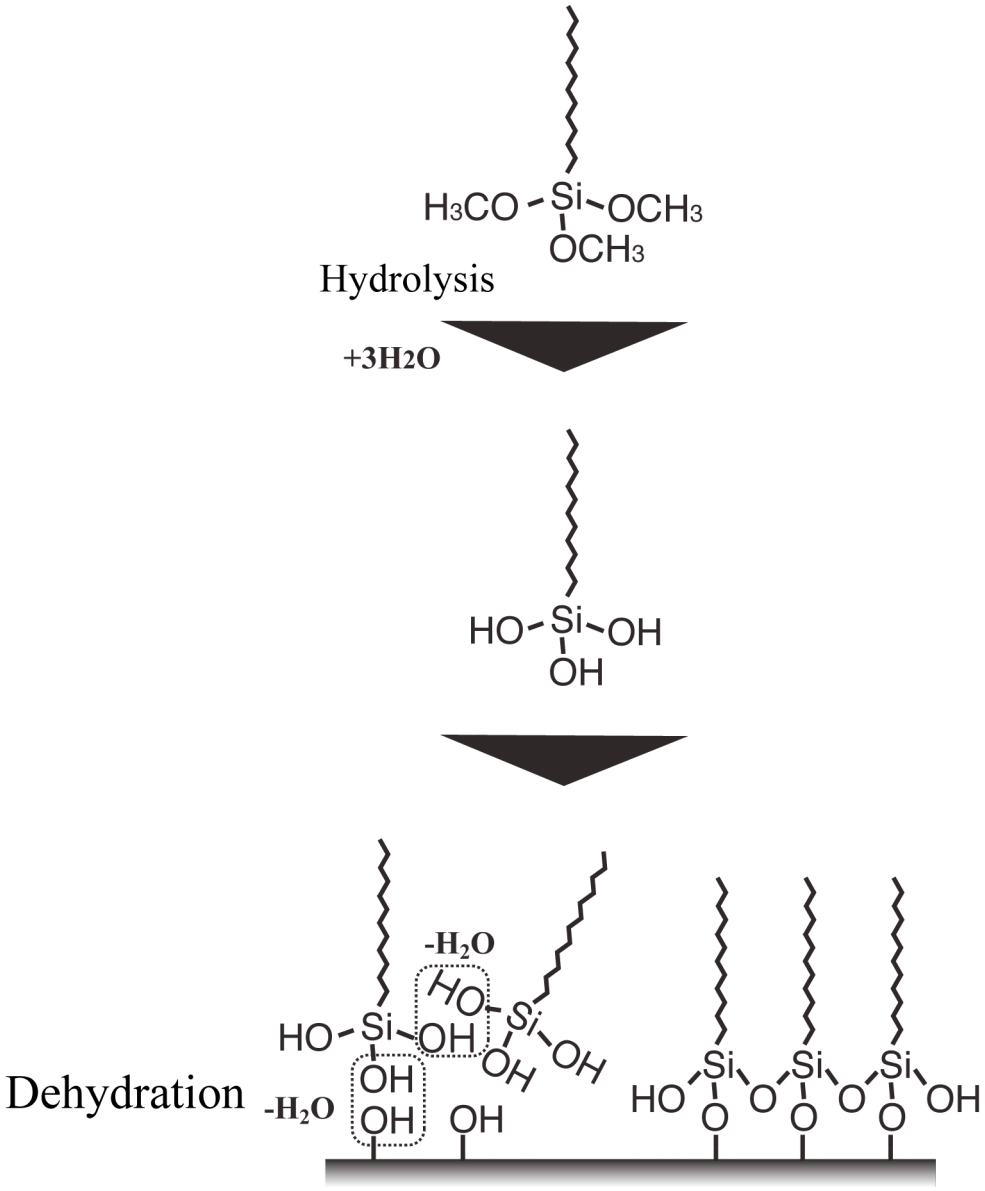

Fig. 3. SAM formation through silane coupling

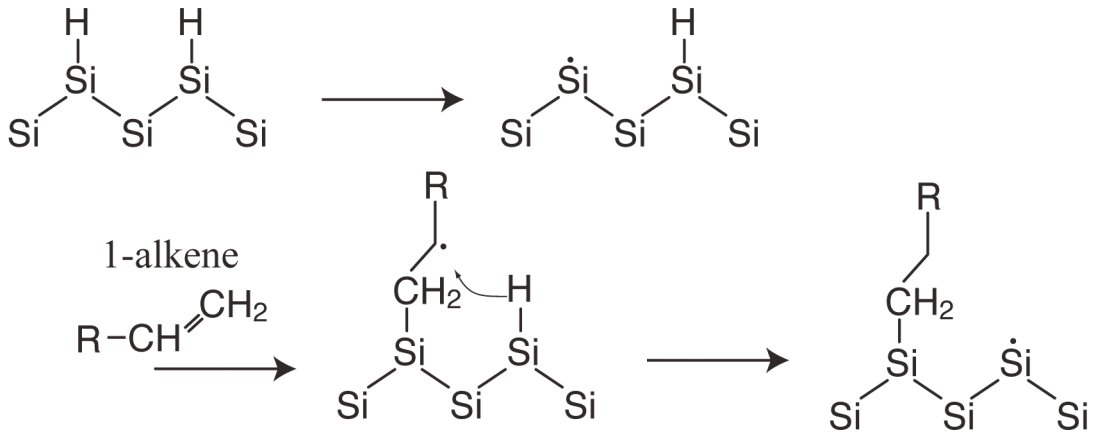

Fig. 4. SAM formation through the radical reaction

1.4.2. SAM directly attached to hydrogen-terminated Si through the radical reaction

SAM directly attached to Si substrates, which is covered with no SiO_2 layers, has been reported in 1993 by Linford et al.[61] The SAM is formed on a hydrogen-terminated Si or halogen-terminated Si substrate through a reaction with organic molecules, such as alkene. Such a reaction is called hydrosilylation. It has been known that the formation of an alkene SAM is done by a radical reaction, through which organic molecules are attracted directly to Si, namely Si-C connection. Figure 4 shows a proposed reaction mechanism. First, a Si radical occur at the sites in which the hydrogen or halogen atoms were drawn out. To produce the radical from each substrate, an initiating reagent injection[61] or a light irradiation[62] was used. The excited radical and the injected molecule react each other, then the molecule combines covalently with the Si atom. At this point, the radical produced newly in the organic molecule pulls out a hydrogen existing on the Si substrate surface, and the radical on the Si substrate is produced newly. As a result, a chain reaction occurs between the molecule and the Si substrate surface. It was also known that the formation of the alkene SAM could be done by heating about 150˚C.[63,64] According to simulation calculation, organic molecules was substituted for hydrogen atom at a rate of 50% in the case of the alkene SAM, if a linear molecule is closely packed on a substrate.[65]

1.5. SPA application to Si substrates covered with SAM

Nanostructures have been successfully fabricated through SPA patterning of SAMs. If combine a SAM with a Si substrate and employ the SAM as a target sample for SPA, we can expect to fabricate a wide variety of nanostructures on Si. Indeed, organosilane SAMs formed on Si substrates have been successfully nanostructured by

SPA and various pattern transfer processes have been demonstrated using a nanostructured SAM as a minute template. For example, SPA-patterned SAMs successfully served as resist masks for wet chemical etching in order to fabricate narrow grooves or minute holes on Si substrates.[66,67] Furthermore, metallic nanostructures consisting of Ni or Au were fabricated on Si surfaces by area-selective electroless plating in which nucleation sites were prepared by a lithographic technique based on SPM and organosilane SAMs.[68-70] Li et al. employed similar nanostructured SAMs as templates in order to assemble Au nanoparticles on specific areas on a SAM-covered Si substrate.[71] Besides metals, organic nanostructures consisting of more than two components have been fabricated as well. For example, a nanostructured sample composed of alkylsilane SAM and Si oxide was first prepared by SPA of the SAM and then the oxide part of the sample surface was area-selectively modified with another organosilane SAM.[53,72] This second SAM was used in order to modify the local surface potential at nanoscale[72] or served as a crosslinker layer on which polymer nanoparticles or biomolecules were area-selectively immobilized.[53] Meanwhile, Sagiv and co-workers developed another SPM-based method to fabricate organic nanostrucures.[45,73] An organic molecular bilayer was self-assembled into a localized area on an organosilane SAM surface of which the top surface functional groups had been converted to be chemically active by SPM tip-induced local anodization. Recently, alkyl SAMs directly attached to Si substrates have attracted attention as a resist for SPA, due to stable and strong Si-C bonding.[74-76] Furthermore, the direct-attach SAM/Si sample provide advantage of very flat surface, which helps SPA to be more successful patterning technologies.

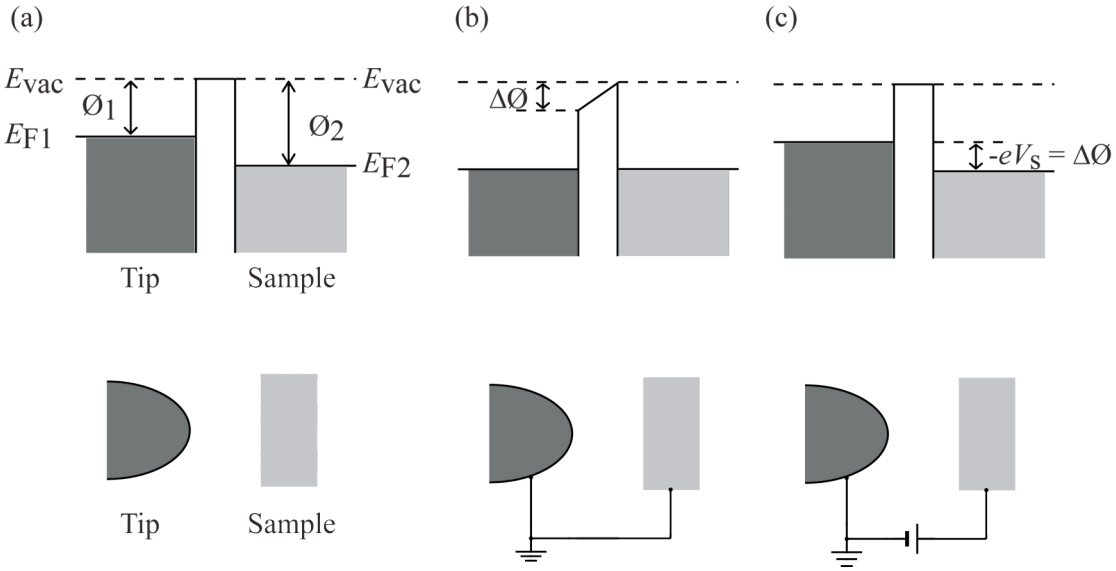

Fig. 5. Band diagrams and corresponding schematic image.

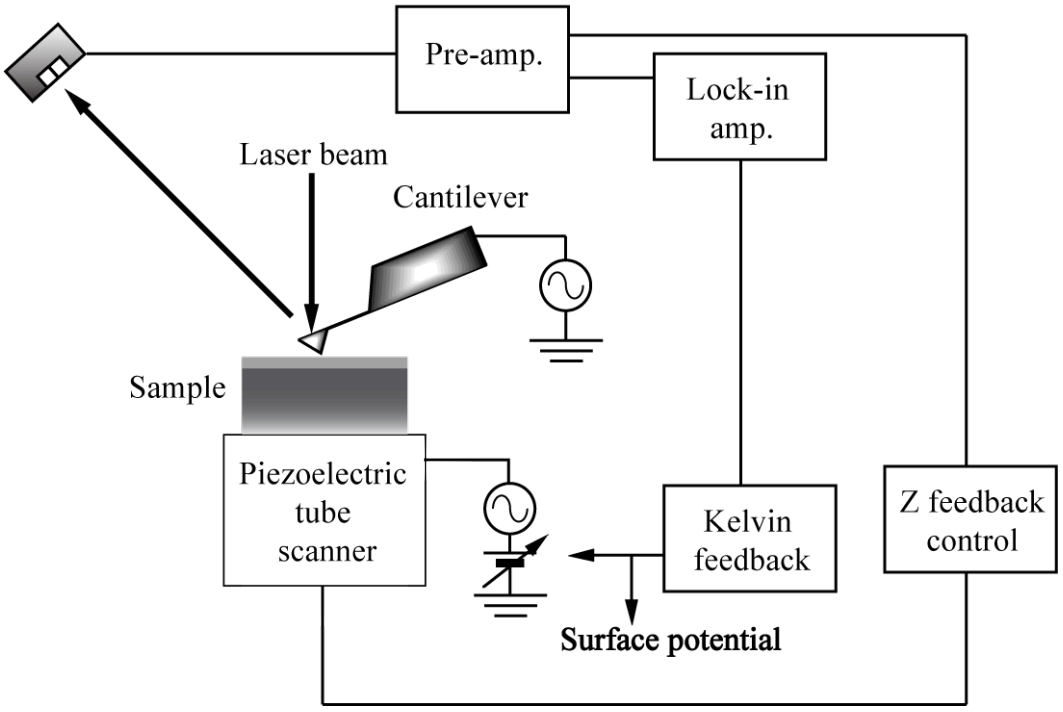

Fig. 6. Schematic of the KFM system.

1.6. Kelvin-probe force microscopy (KFM)

The KFM is a modified system of the AFM, which measure local surface potential differences.[13,14] The principle of KFM is explained as follows.[77] Let us consider that the band diagrams of different work function materials and corresponding KFM schematic images are shown in Fig. 5. Work function of each material is supposed to include it′s change by any materials absorbed on the tip and sample surface. Suppose vacuum level between the tip and the sample is equal as shown in Fig 5a. When the tip and the sample is connected each other as shown in Fig. 5b, the Fermi level of both the tip and the sample is equal, and contact potential difference (CPD) $V_{CPD} = \Delta\phi = (\phi_1 - \phi_2)/e$ occurs, where ϕ_1 is the tip work function, ϕ_2 the sample work function, e the electron. At this point, when modulated bias voltage $V_m = V_{DC} + V_{AC}\cos(\omega_m t)$ is applied, electrostatic force $F_{ele} = -\frac{1}{2}\frac{\partial C_{ts}}{\partial_z} V^2{}_{CPD}$ between the tip and the sample surface is written as

$$F_{ele} = -\frac{1}{2}\frac{\partial C_{ts}}{\partial_z}(V_m + V_{CPD})^2 \qquad (1\text{-}1)$$

$$= -\frac{1}{2}\frac{\partial C_{ts}}{\partial_z}\left\{(V_{DC} + V_{CPD})^2 + 2(V_{DC} + V_{CPD})V_{AC}\cos(\omega_m t) + V^2{}_{AC}\cos^2(\omega_m t)\right\} \qquad (1\text{-}2)$$

$$= -\frac{1}{2}\frac{\partial C_{ts}}{\partial_z}\left[\left\{(V_{DC} + V_{CPD})^2 + \frac{1}{2}V^2{}_{AC}\right\} + 2(V_{DC} + V_{CPD})V_{AC}\cos(\omega_m t) + \frac{1}{2}V^2{}_{AC}\cos^2(2\omega_m t)\right] \qquad (1\text{-}3)$$

where V_{DC} is the dc voltage, V_{AC} the ac modulation voltage, ω_m the modulated angular frequency, C the tip-sample capacitance. In Eq. (1.3), the dc, ω_m, and $2\omega_m$ are the electrostatic force component. With only electrostatic force component ω_m noticed, the equation is written as

$$(F_{ele})_m = -\frac{\partial C_{ts}}{\partial_z}(V_{DC} + V_{CPD})V_{AC}\cos(\omega_m t) \quad (1\text{-}4)$$

In order to satisfy $V_{DC} + V_{CPD} = 0$, CPD is nullified by applying a dc voltage to the sample. Vacuum level both of the tip and the sample therefore becomes the same, and electrostatic force $(F_{ele})_m$ is zero as shown in Fig. 5c. This electrostatic force $(F_{ele})_m$ is detected by Lock-in technique, and a Kelvin feedback system adjusts the dc bias voltage until ω_m component is nullified, as shown in Fig. 6, which is a general KFM system. As a result, such a voltage $-V_{DC}$ mapping is imaged as a surface potential difference, namely CPD.

1.6. Scanning capacitance microscopy (SCM)

The SCM also is a modified system of the AFM, which measure a differential capacitance.[15,16] The principle of SCM is explained as follows. The conductive tip contacts with Si semiconductor device covered with SiO_2 layer, as shown in Fig. 7a. This structure is similar with Metal insulator semiconductor (MIS) structure shown Fig. 7b. The operating principle of SCM therefore is based on the MIS operating principle, in which the conductive tip works as the gate metal. Figure 8 shows energy band diagram for n-type semiconductor biased with positive or negative voltages from a gate metal. When a positive voltage is applied to the gate metal, the conduction band (E_c) bends downside (Fig. 8a). This band bending causes an accumulation of electrons near semiconductor surface. When a negative voltage is applied, the conduction band bends upside (Fig. 8b). This bending causes a depletion of electrons. When a larger voltage is applied, the band bends further more upside so that the intrinsic level (E_I) near the surface crosses the Fermi level (E_F) (Fig. 8c). Therefore, the surface is inverted because the number of holes near the surface is larger than that

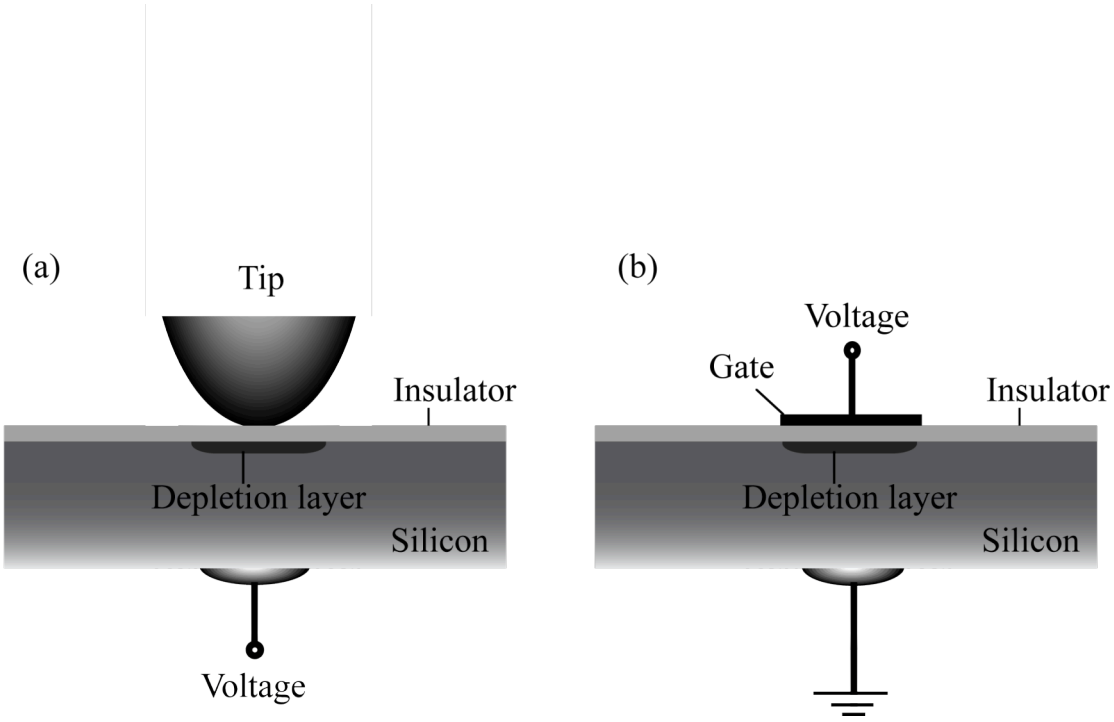

Fig. 7. (a) MIS structure formed by the SPM tip, (b) MIS structure formed by the gate

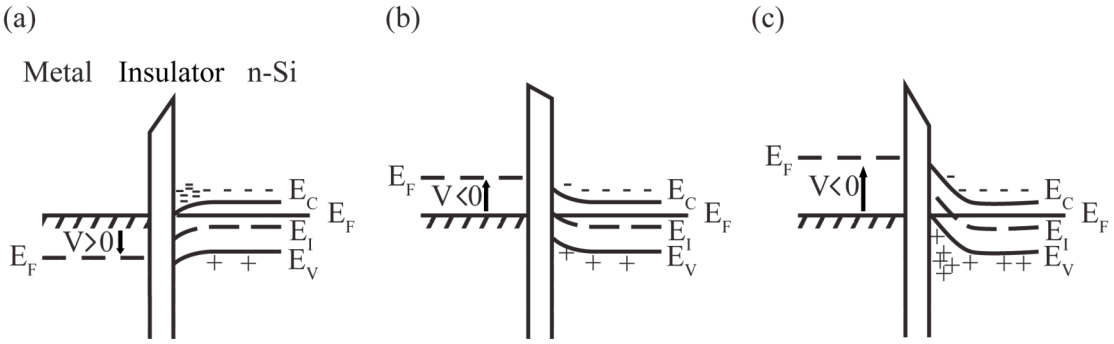

Fig. 8. Energy band diagrams for MIS (n-type) structures, (a) accumulation, (b) depletion, (c) inversion.

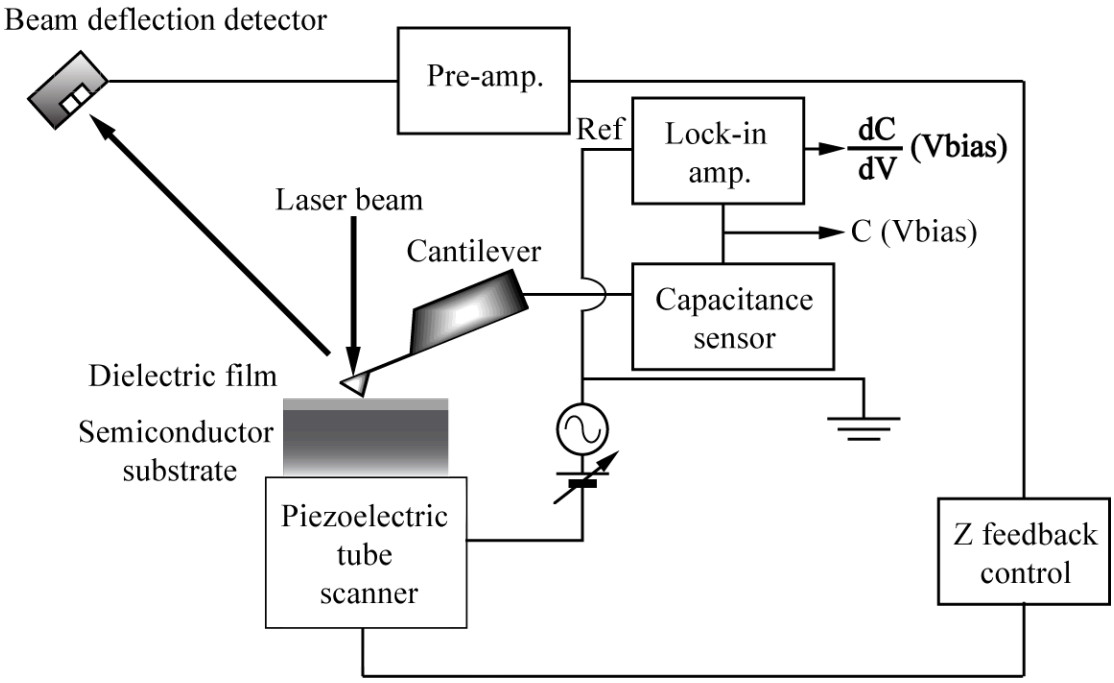

Fig. 9. Schematic of the SCM system.

of the electrons. These phenomena also occur in the SCM measurement. For the accumulation case, SCM only observes differential oxide capacitance, due to an existing electron under oxide layer. For the depletion case, SCM observes differential oxide and depletion-layer capacitance. For the inversion case, SCM only observes differential insulator capacitance, because the depletion-layer width does not change by applied ac voltage. Figure 9 shows a schematic of the SCM system. SCM measures differential capacitance (dC/dV) at a superimposing ac signal on an applied dc voltage by capacitance sensor connected to the cantilever, not capacitance (C). A Lock-in amplifier can observe the change of the amplitude and the phase in capacitance signal at applied ac and dc voltage. Therefore, the resulting lock-in shows the slope of C-V curve, namely (dC/dV) at the applied dc voltage. As a result, such a differential capacitance (dC/dV) mapping at the applied dc voltage is shown as a SCM image. Figure 10 shows the general C-V curve and dC/dV-V curve for n-type semiconductors samples using scanning capacitance spectroscopy (SCS). The curve is obtained as explained in the SCM operating principles. But we must notice bias voltages are applied to the sample, not the tip, in our SCM system. Increasing bias voltages to the sample produce depletion layer underneath an insulator layer, then the capacitance value between the tip and the insulator is reduced. As a result, the capacitance becomes constant. These changes are detected and shown as dC/dV-V curve in the SCM system. In the case of p-type Si sample, an opposite phenomenon occurs. On the other hand, trapped charges in the insulator cause the shift of a dC/dV-V curve peak. Positive and negative trapped charges in the insulator cause the negative and the positive shift of a dC/dV-V curve peak with respect to the ideal peak, which means no charge trap in the insulator. These charges therefore can be detected by SCS.

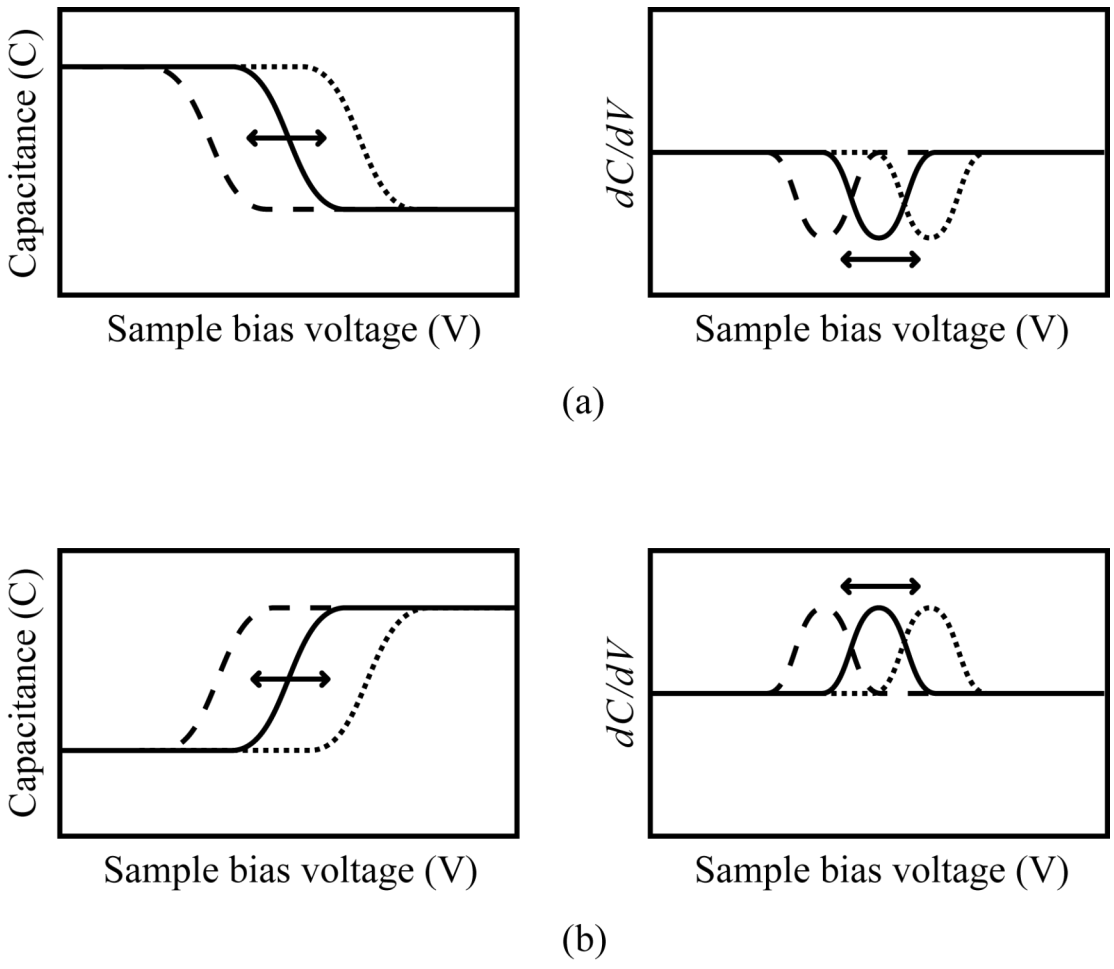

Fig. 10. General C-V and dC/dV-V curve. (a) For n-type semiconductor, (b) For p-type semiconductor

References

1) G. Binnig, H. Rohrer, Ch. Gerber, and E. Weibel, Phys. Rev. Lett. **49** (1982) 57.

2) G. Binnig, C. F. Quate, and Ch. Gerber, Phys. Rev. Lett. **56** (1986) 930.

3) J. A. Dagata, J. Schneir, H. H. Harary, C. J. Evans, M. T. Postek, and J. Bennett, Appl. Phys. Lett. **56** (1990) 2001.

4) L.A. Nagahara, T. Thundat, S. M. Lindsay, Appl. Phys. Lett. **57** (1990) 270.

5) H. Sugimura, T. Uchida, N. Kitamura, and H. Masuhara, Jpn. J. Appl. Phys. **32** (1993) L553.

6) R. Magno and B. R. Bennett, Appl. Phys. Lett. **70** (1997) 1855.

7) R. D. Piner, J. Zhu, F. Xu, S. Hong, and C. A. Mirkin, Science **283** (1999) 661.

8) J. Zhao and K. Uosaki, Nano Lett. **2** (2002) 137.

9) R. L. McCarley, S. A. Hendricks, and A. J. Bard, J. Phys. Chem. **96** (1992) 10089.

10) H. Sugimura, T. Uchida, N. Kitamura, and H. Masuhara, J. Phys. Chem. **98** (1994) 4352.

11) A. Ulman, An Introduction to Ultrathin Organic Films from Langmuir-Blodgett to Self-Assembly (Academic press, London, 1991).

12) 山口克彦，材料加工プロセス，共立出板株式会社 (2006).

13) M. Nonnenmacher, M. P. O'Boyle, and H. K. Wickramasinghe, Appl. Phys. Lett. **58** (1991) 2921.

14) 森田清三，原子·分子のナノ力学， 丸善株式会社 (2003).

15) C. C. Williams, W. P. Hough, and S. A. Rishton, Appl. Phys. Lett. **55** (1989) 203.

16) Y. Cho, S. Kazuta and K. Matsuura, Appl. Phys. Lett. **75** (1999) 2833.

17) R. C. Barrett and C. F. Quate, J. Appl. Phys. **70** (1991) 2725.

18) W. Brezna, S. Harasek, E. Bertagnolli, E. Gornik, J. Smoliner, and H. Enichlmair,

J. Appl. Phys. **92** (2002) 2144.

19) M. A. Salem, H. Mizuta, and S. Oda, Appl. Phys. Lett. **85** (2004) 3262.

20) J. Cermak, A. Kromka, and B. Rezek, Phys. Stat. Sol. (a) **205** (2008) 2136.

21) N. Saito, S. Youda, K. Hayashi, H. Sugimura, and O. Takai, Chem. Lett. **31** (2002) 1194.

22) M. C. Daniel and D. Astruc, Chem. Rev. **104** (2004) 293.

23) G. Schmid and U. Simon, Chem. Commun. (2005) 697.

24) P. Avoris, Acc. Chem. Res. **28** (1995) 95.

25) R. M. Nyffebegger and R. M. Penner, Chem. Rev. **97** (1997) 1195.

26) C. F. Quate, Surf. Sci. **386** (1997) 259.

27) D. Wouters and U. S. Schubert, Angew. Chem. Int. Ed. **43** (2004) 2480.

28) M. A. McCord, D. P. Kern, and H. P. Chang, J. Vac. Sci. Technol. B **6** (1988) 1877.

29) C. R. K. Marrian and R. J. Colton, Appl. Phys. Lett. **56** (1990) 755.

30) Y. Okawa and M. Aono, Nature **409** (2001) 683.

31) H. Kuramochi, H. Uchida, and M. Aono, Phys. Rev. Lett. **72** (1994) 932.

32) B. J. McIntyre, M. Salmeron, and G. A. Somorjai, Science **265** (1994) 1415.

33) W. T. Müler, D. L. Klein, T. Lee, J. Clarke, P. M. McEuen, and P. G. Schultz, Science **268** (1995) 272.

34) C. Blackledge, D. A. Engebretson, and J. D. McDonald, Langmuir **16** (2000) 8317.

35) S. Takeda, C. Nakamura, C. Miyamoto, N. Nakamura, M. Kageshima, H. Tokumoto, and J. Miyake, Nano Lett. **3** (2003) 1471.

36) M. Péter, X.-M. Li, J. Huskens, and D. N. Reinhoudt, J. Am. Chem. Soc. **126** (2004) 11684.

37) T. Thundat, L. A. Nagahara, P. 1. Oden, S. M. Lindsay, M. A. George, and W. S. Glaunsinger, J. Vac. Sci. Techno1. A **8** (1990) 3537.

38) H. C. Day and D. R. Allee, Appl. Phys. Lett. **62** (1993) 2691.

39) E. S. Snow, P. M. Campbell, and P. J. MacMarr, Appl. Phys. Lett. **63** (1993) 749.

40) H. Sugimura, T. Uchida, N. Kitamura, and H. Masuhara, Jpn. J. Appl. Phys. **33** (1994) L143.

41) T. Kondo, M. Yanagisawa. L. Jiang, D. A. Tryk, and A. Fujishima, Dia. Relat. Mater. **11** (2002) 1788.

42) E. S. Snow. D. Park. and P. M. Campbell, Appl. Phys. Lett. **69** (1996) 269.

43) K. Watanabe, Y. Takemura, Y. Shimazu, and J. Shirakashi, Nanotechnology **15** (2004) S566.

44) H. J. Song, M. J. Rack, K. Abugharbieh, S. Y. Lee, V. Khan, D. K. Ferry, and D. R. Allee, J. Vac. Sci. Technol. B. **12** (1994) 3720.

45) R. Maoz, S. R. Cohen, and J. Sagiv, Adv. Mater. **11** (1999) 55.

46) Y.-H. Kim, J. Zhao, and K. Uosaki, J. Appl. Phys. **94** (2003) 7733.

47) A. Avramescu, A. Ueta, K. Uesugi, and I. Suemune, Appl. Phys. Lett. **72** (1998) 716.

48) H. Sugimura and N. Nakagiri, Langmuir **10** (1995) 3623.

49) S. J. Ahn, Y. K. Jang, and H. Lee, Appl. Phys. Lett. **80** (2002) 2592.

50) D. A. Grigg, P. E. Russell, and J. E. Griffith, J. Vac. Sci. Technol. B **10** (1992) 680.

51) B. L. Weeks and M. W. Vaughn, Langmuir **21** (2005) 8096.

52) S. Britland, E. Perez-Arnaud, P. Clark, B. McGinn, P. Connolly, and G. Moores, Biotechnol. Prog. **8** (1992) 155.

53) H. Sugimura and N. Nakagiri, J. Am. Chem. Soc. **119** (1997) 9226.

54) R. K. Smith, P. A. Lewis, and P. S. Weiss, Prog. Surf. Sci. **75** (2004) 1.

55) A. Facchetti, M.-H. Yoon, and T. J. Marks, Adv. Mater. **17** (2005) 1705.

56) B. R. Murthy, W. M. Yee, A. Krishnamoorthy, R. Kummar, and D. C. Frye, Electrochem. Solid-state lett. **9** (2006) F61.

57) J. Zheng, Z. Zhu, H. Chen, and Z. Liu, Langmuir **16** (2000) 4409.

58) J. C. Garno, C. D. Zangmeister, and J. D. Batteas, Langmuir **23** (2007) 7874.

59) E. E. Polymeropoulos and J. Sagiv, J. Chem. Phys. **69** (1978) 1836.

60) J. Sagiv, J. Am. Chem. Soc. **102** (1980) 92.

61) M. R. Linford and C. E. D. Chidsey, J. Am. Chem. Soc. **115** (1993) 12631.

62) F. Effenberger, G. Götz, B. Bidlingmaier, and M. Wezstein, Angew. Chem. Int. Ed. **37** (1998) 2462.

63) M. R. Linford, P. Fenter, P. M. Eisenberger, and C. E. D. Chidsey, J. Am. Chem. Soc. **117** (1995) 3145.

64) M. M. Sung, G. J. Kluth, O. W. Yauw, and R. Maboudian, Langmuir **13** (1997) 6164.

65) A. B. Sieval, B. van den Hout, H. Zuilhof, and E. J. R. Sudhoelter, Langmuir, **16** (2000) 2987.

66) H. Sugimura, K. Okiguchi, and N. Nakagiri, Jpn. J. Appl. Phys. **35** (1996) 3749.

67) H. Sugimura, T. Hanji, K. Hayashi, and O. Takai, Ultramicroscopy **91** (2002) 221.

68) C. R. K. Marrian, F. K. Perkins, S. L. Brandow, T. S. Koloski, E. A. Dobisz, and J. M. Calvert, Appl. Phys. Lett. **64** (1994) 390.

69) S. L. Brandow, J. M. Calvert, E. S. Snow, and P. M. Campbell, J. Vac. Sci. Technol. A **15** (1997) 1455.

70) H. Sugimura, O. Takai, and N. Nakagiri, J. Electroanal. Chem. **473** (1999) 230.

71) Q. Li, J. Zheng, and Z. Liu, Langmuir **19** (2003) 166.

72) H. Sugimura, T. Hanji, K. Hayashi, and O. Takai, Adv. Mater. **14** (2002) 524.

73) S. Hoeppener, R. Maoz, S. R Cohen, L. Chi, H. Fuchs, and J. Sagiv, Adv. Mater. **14** (2002) 1036.

74) M. Ara, H. Graaf, and H. Tada, Appl. Phys. Lett. **80** (2002) 2565.

75) B. Pignataro, A. Licciardello, S. Cataldo, G. Marletta, Mater. Sci. Eng. C **23** (2003) 7.

76) Y. Menglong, Z. Zhikun, L. Yaqing, and Z. Bailin, Nanotechnology **17** (2006) 330.

77) 一井 崇，周波数変調方式ダイナミックフォース顕微鏡を用いた有機超薄膜の分子スケール構造・物性評価，博士論文，京都大学 (2006).

2. Effect of relative humidity, hydrophilicity, and tip material on SPA

Nanostructuring Si surfaces is of primary importance for micro ~ nano electronics. SPM-based nanofabrication techniques have been successfully applied for Si nanopatterning. Among various SPM patterning methods based on a characteristic surface modification mechanism, the localized oxidation of a material surface has been most widely studied so far.[1)] In particular, the generation of anodic electrochemical reactions in an adsorbed water meniscus at an SPM tip-sample junction, which is attained by operating the SPM in a humid atmosphere and applying a positive sample bias,[2-5)] has become a promising SPM nanofabrication principle because of its advantages, for example, the applicability to a wide variety of substrate materials including Si. First, this method was directly applied to Si substrates. Then it was extended to Si surfaces covered with an organic resist film such as SAMs and spin-coated polymer films for the fabrication of minute structures on Si.[6-9)]

Alkyl SAMs directly attached to Si substrates typically through Si-C bonds have attracted attention as alternatives to organosilane SAMs,[10)] because of their atomically flat surfaces,[11] thermal and chemical stability[12,13)] and a similar patternability in SPA.[14-16)] The direct-attach SAM/Si sample can be anodized with a lower threshold bias than that for an organosilane SAM/Si sample which has an interfacial oxide layer at least 2 nm in thickness.[15,16)] Charge traps which degrade the performance of Si electronic devices have been found to be not present at the SAM-Si interface, in contrast to the organosilane SAM/Si samples.[17)]

Although SPA has been successfully applied to nanopatterning of the direct-attach SAM/Si samples so far, there have been few studies from the view point of the size control of the adsorbed water meniscus formed at the SPM-tip/sample junction in spite of its particular influence on the patterning resolution. In this study, therefore,

we focused on the effects of relative humidity (RH), surface hydrophilicity of SAMs and probe-tip materials on SPA of SAM-Si samples.

2.1. Experimental procedure

2.1.1. Formation of SAMs directly attached to Si

Three types of SAM-covered Si samples were prepared for this work. Prior to the SAM formation, Si substrates cut from an n-type Si (111) wafer with a resistivity of 1 - 10 Ω cm were cleaned by sonication in ethanol and ultrapure water, in that order, for 20 min, respectively. Then, carbonaous contamination on the Si substrates was removed by a photochemical method using a light source radiating vacuum ultra violet at 172 nm in wavelength (Ushio UER20-172V; intensity at the lamp window, 10mW cm^{-2}). The details of this photochemical cleaning method are described elsewhere.[18] Next, in order to remove surface oxide, cleaned Si substrates were treated in 5 % HF aqueous solution for 5 min at room temperature (RT) followed by 40 % NH_4F aqueous solution for 30 sec at 80˚C so that the Si substrate surfaces became terminated with hydrogen. Finally, onto each of these Si(111)-H substrates, a SAM was formed by a thermal activation method.[19] One of the Si-H samples was placed in a three-neck separable glass flask filled with 1M solution of 1-undecene in mesitylene kept at 150˚C for 2 hours. The inside of the flask was purged with N_2 bubbling, as illustrated in Fig. 1. Consequently, an undecyl SAM, which is terminated with methyl groups, was formed on the substrate. Similarly, an ester-terminated SAM was formed in 1M solution of 10-undecenoic acid methyl ester in mesitylene on each of the other Si-H substrates. After the SAM formation processes, all the samples were rinsed by sonication in mesitylene, ethanol, and ultrapure water for 5 min each, in that order, and then dried in a stream of N_2 gas. A sample coated with a carboxyl-

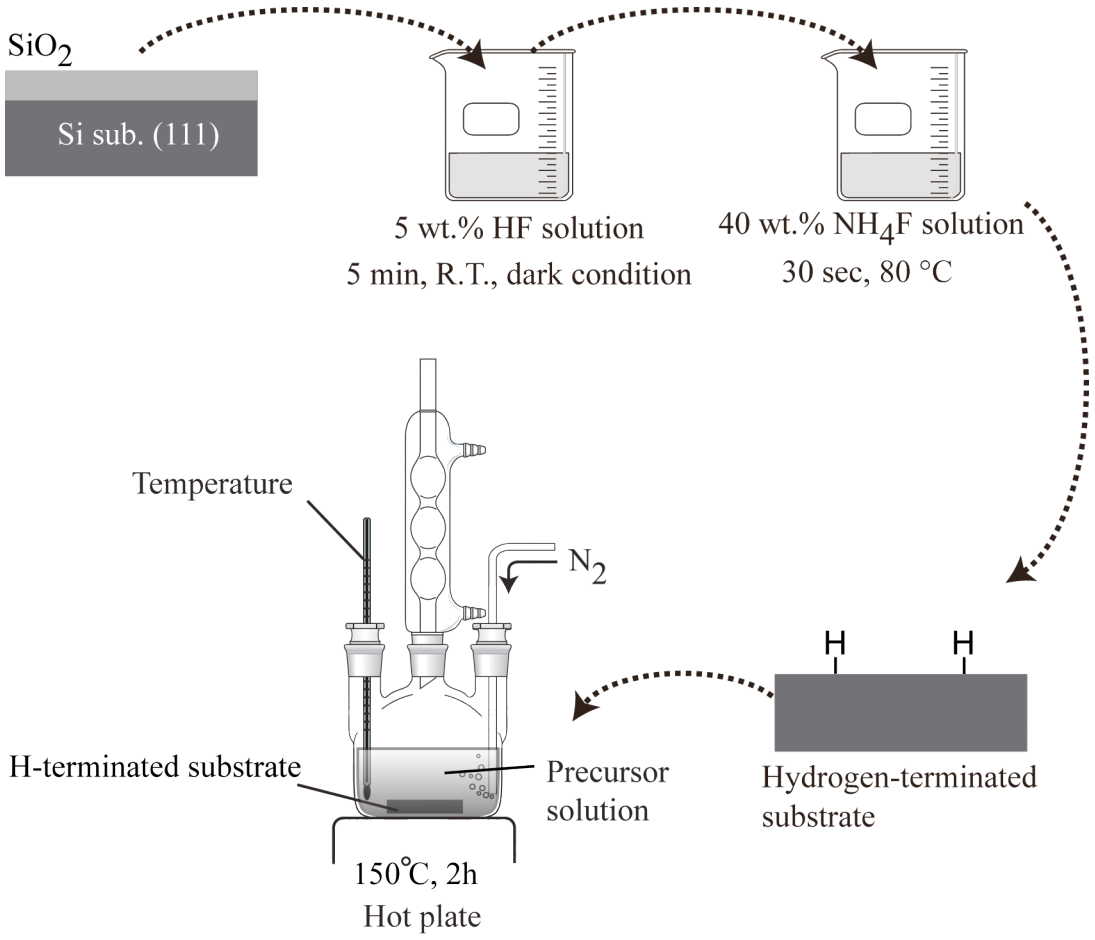

Fig. 1. Schematic illustration of the process of the SAM directly attached to Si (111) plane by a thermal activation

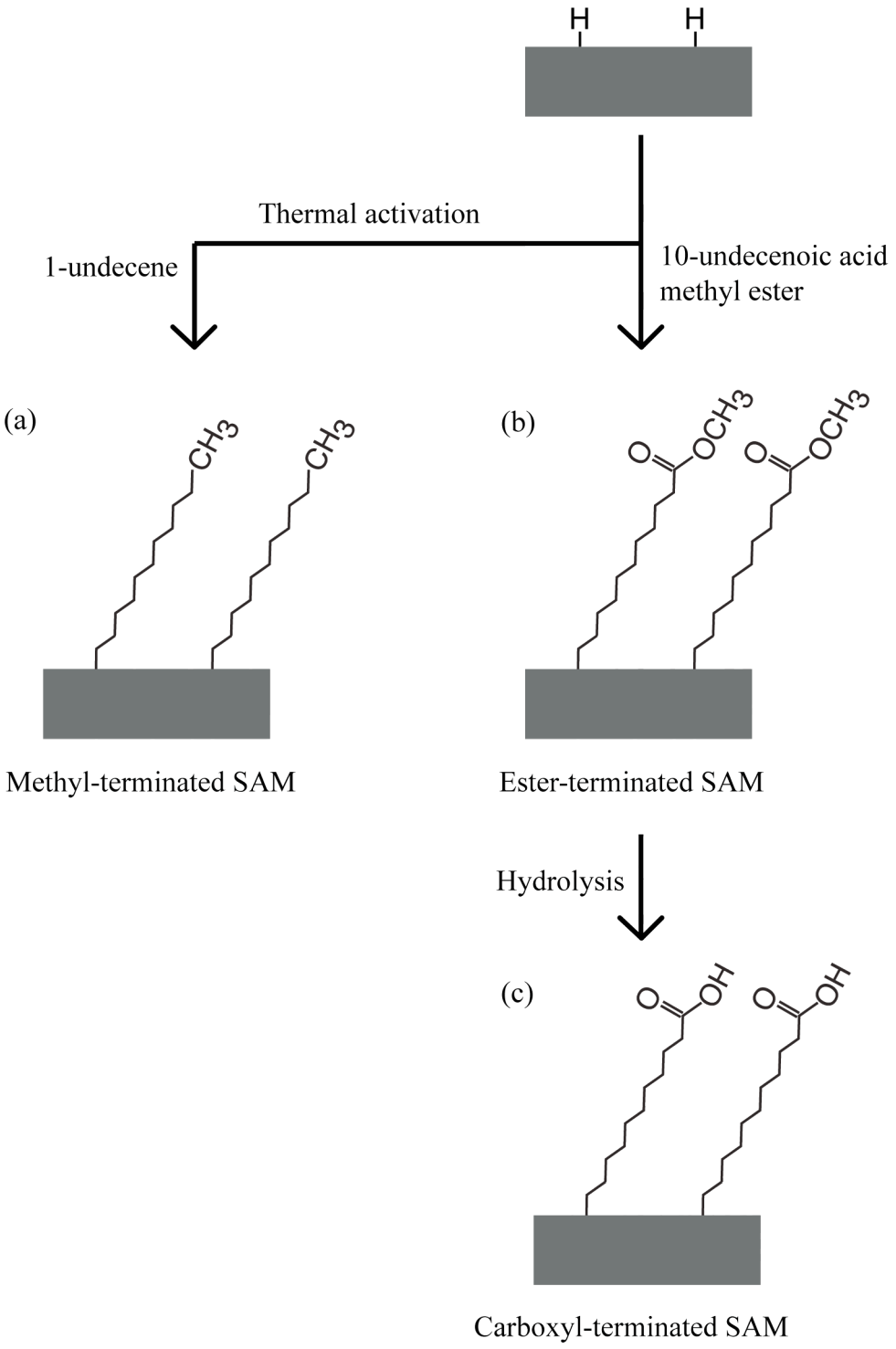

Fig. 2. Schematic illustration of the sample preparation procedures. (a) methyl-terminated SAM, (b) ester-terminated SAM, and (c) carboxyl-terminated SAM.

terminated SAM was obtained by hydrolysis of the surface ester groups on the ester-terminated SAM. This process was conducted by treating the sample with a 0.25 M solution of potassium *tert*-butoxide in dimethyl sulfoxide for 10 min at RT, and with a 1 M HCl for 10 min at RT. After the treatment, the sample was sonicated in ultrapure water for 5 min and then dried in a stream of N_2 gas.[20,21] Schematic illustration of the sample preparation is shown in Fig. 2. Water contact angles (Kyowa Interface Science, CA-X) of the methyl-, ester-, and carboxyl-terminated SAMs were approximately 96°, 73°, and 53°, respectively. The thicknesses of the SAMs were all approximately 1.8 nm as measured by ellipsometry (Otsuka Electronics, FE-5000). The conversion of ester to carboxyl was monitored by quantitative fourier transform infrared spectroscopy (FTIR; Digilab Japan Co., Ltd, Excalibur FTS-3000) as shown in Fig. 3. The FT-IR results of a transmittance mode showed evidence for the conversion of ester to carboxyl group. Because the peak position at 1749 cm^{-1} and 1721 cm^{-1} are assigned to ester group and carboxyl group, respectively.

2.1.2. SPM processes

Patterning experiments were performed using a commercial AFM (SII NanoTechnology Inc., SPA-300HV + SPI-3800N) in contact mode under controlled atmospheric humidity. Figure 4 shows the humidity controller consisting of three bottles, two regulators, and two hygrometers. Among bottles, two contained water and the other was empty. Air saturated with water vapor and dry air streamed into a big bottle, then the RH in the big bottle was monitored. The controlled air was flown to a chamber where the AFM unit was located. The RH in the chamber was also

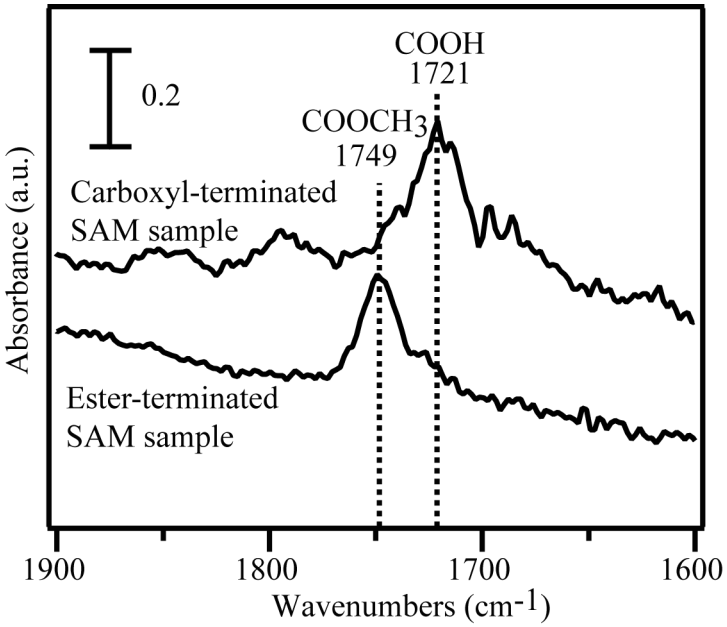

Fig. 3. Transmission IR spectra of Si substrates modified with ester and carboxyl-terminated group

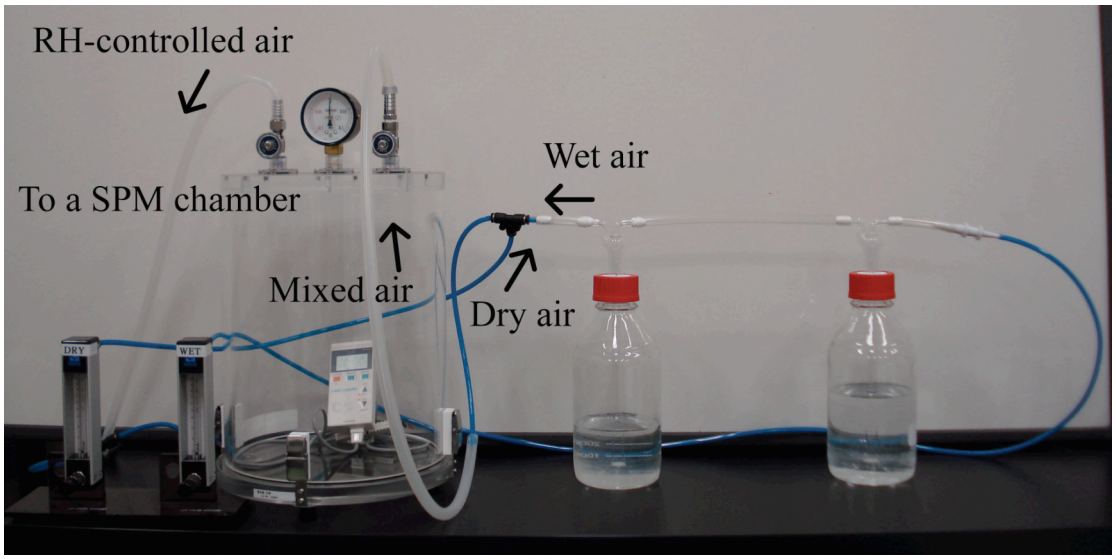

Fig. 4. Humidity controlling system

monitored through small hole of the chamber. The RH was adjusted through the flow rate of each gas stream, from 10 to 70 %. The RH in the AFM chamber was monitored with 3% error in the range of 0 to 90% RH at room temperature by a precision hygrometer (MR6662, Chino, Japan). In this experiment, 10, 40, and 70% RH were subsequently adjusted at one-hour intervals for patterning. A sample bias voltage relative to the grounded probe tip was applied to the substrate Si of a SAM-covered sample. The probe was scanned at a scan rate of 0.5 μm/s with a bias of 10 V under a controlled RH of 10%, 40%, or 70% RH at a temperature of 17 ± 2˚C. Either a Rh-coated Si tip (Rh-tip: SII NanoTechnology Inc., SI-DF3-R, force constant of 1.6 N/m, resonance frequency of 26 kHz and tip radius of about 30 nm) or a boron-doped conductive diamond-coated tip (CDT: Nano sensor, CDT-FMR, force constant of 2.2 N/m, resonance frequency of 75 kHz and tip radius of about 100 nm) was used for the patterning. After patterning, topographic AFM images of the patterned samples were acquired in dynamic mode using a Si probe tip (SII NanoTechnology Inc., SI-DF20-Al, force constant of 12 N/m, resonance frequency of 125 kHz and tip radius of about 15 nm) under a N_2 purged atmosphere.

In order to investigate the relative water meniscus sizes formed at the tip-sample junction under the patterning condition, we performed force curve measurements while applying a tip-sample voltage of 10 V. As shown in Fig. 5, the pull-off force demonstrates a maximum attractive force when the AFM tip is retracted from the sample surface. Force curves were taken at ten different positions on the ester-SAM sample surface using the Rh-tip or the CDT, in order to avoid effects of any topographical change produced due to the previous force curve measurements. The AFM probe was scanned along the z-direction at a rate of 70 nm/s. The RH value in the chamber was controlled in the same way as during the patterning.

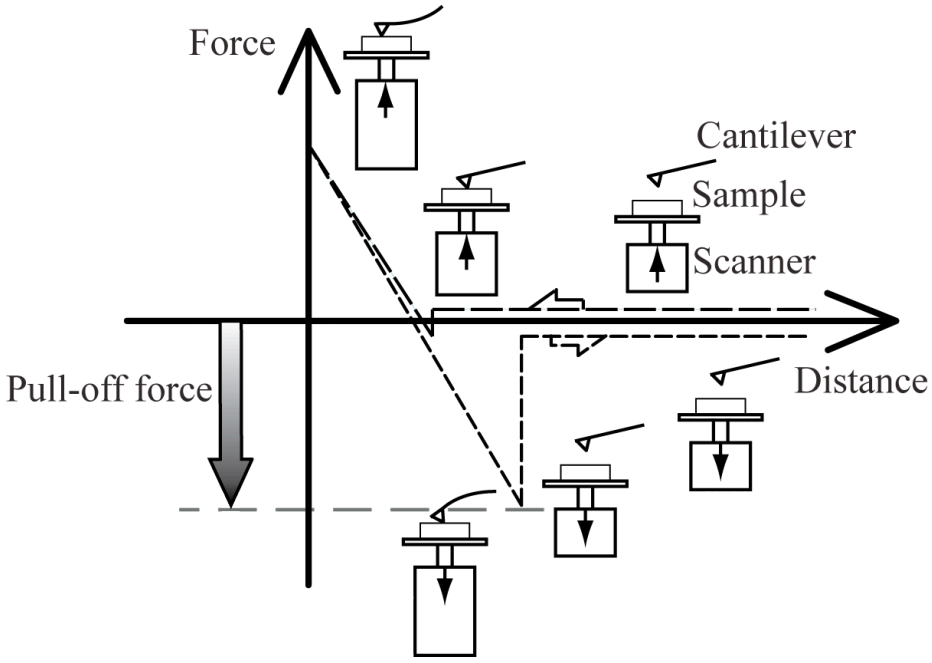

Fig. 5. Schematic diagram of force-distance curve.

2.2. Results and discussion

Figure 6 shows AFM images of fabricated lines on the samples. Protruded lines are seen in all the images. On SPA of a SAM-covered Si sample with a constant bias voltage, organic molecules consisting of the SAM are, first, gradually decomposed, and accordingly, the SAM is degraded. However, in the initial stage the substrate Si does not react at all since the electrochemical species necessary for anodization of Si are almost perfectly blocked by the SAM itself. When the SAM is degraded to some extent due to anodization, the electrochemical species start to reach into the substrate Si, and it begins to be anodized. In the final stage, the decomposition of the SAM is completed if the bias is sufficient. In this stage, only anodization of the substrate Si proceeds until the thickness of the anodic oxide reaches a specific value determined mainly by the bias voltage for anodization.[22,23] Finally, due to the larger specific volume of Si oxide than Si, a protruded line is fabricated along the tip-scan trace where anodic Si oxide has been formed.

2.2.1. Topographical change in anodized lines by the Rh-coated Si tip

Figures 6(a)-(c) show lines fabricated on the methyl-terminated SAM (methyl-SAM) sample using a Rh-tip at RH = 10, 40 and 70%, respectively. The line width increases from 25 nm (10% RH) to 105 nm (70% RH). Figures 6(d)-(f) indicate lines fabricated on the ester-terminated SAM (ester-SAM) sample using the same Rh-tip at RH = 10, 40 and 70%, respectively. The line width increases from 20 nm (10% RH) to 140 nm (70% RH). The results on the carboxyl acid-terminated SAM (carboxyl-SAM) sample are shown in Figs. 6(g)-(i). These lines were fabricated at RH = 10, 40 and 70%, respectively, with the same Rh-tip used for the experiments on the methyl-

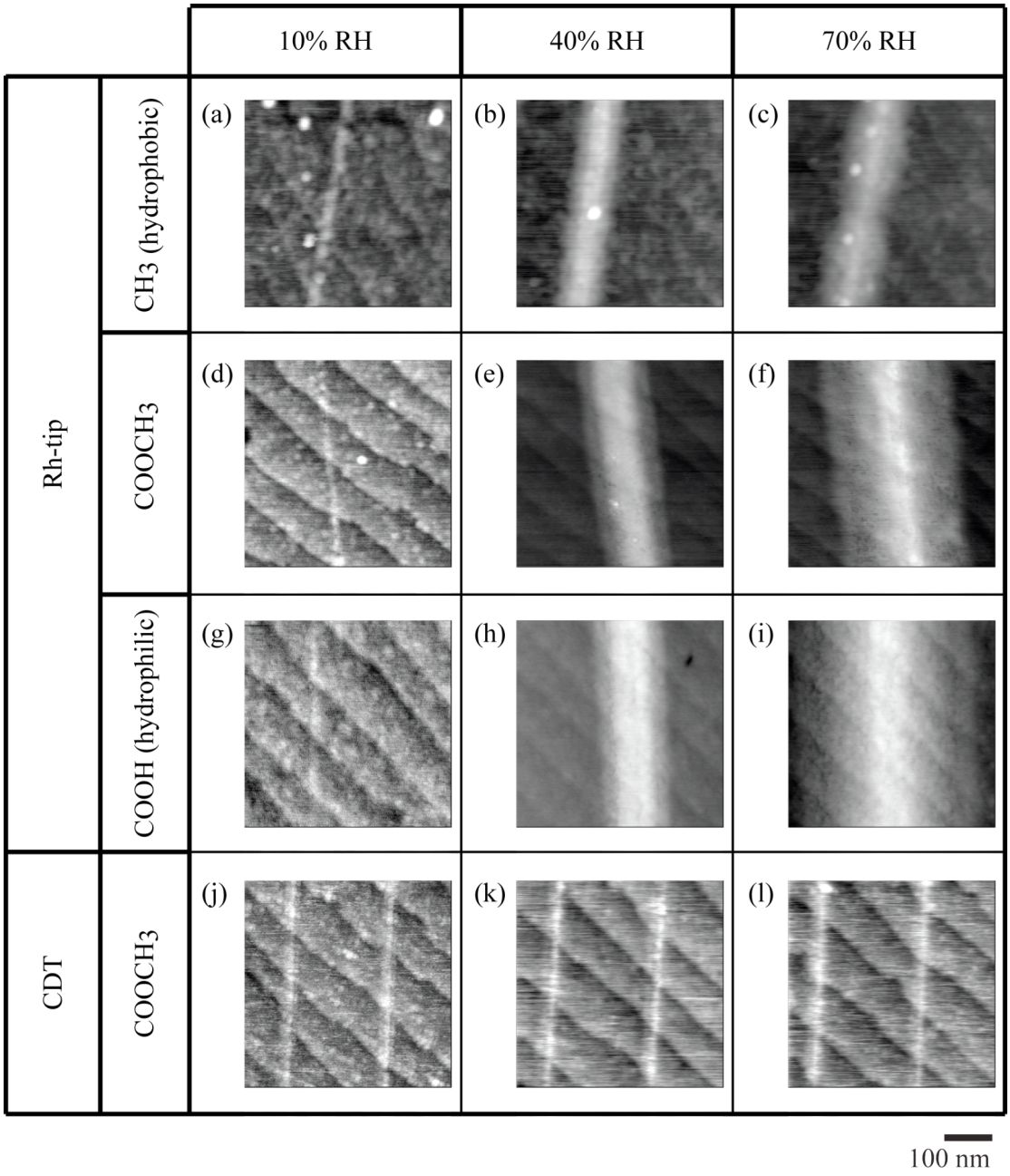

Fig. 6. Topographic images acquired by dynamic-mode AFM for the patterned regions. Fabricated lines on the methyl-SAM sample at RH = (a) 10%, (b) 40% and (c) 70% using the Rh-tip. Fabricated lines on the ester-SAM sample at RH = (d) 10%, (e) 40% and (f) 70% using the Rh-tip. Fabricated lines on the carboxyl-SAM sample at RH = (g) 10%, (h) 40% and (i) 70% using the Rh-tip. Fabricated lines on the ester-SAM sample at RH = (a) 10%, (b) 40% and (c) 70% using the CDT.

and ester-SAM samples. The line width increases from 20 nm (10% RH) to 230 nm (70% RH).

The widths (full width at half maximum) and heights of the lines are summarized in Fig. 7. These values were estimated from ten section profiles of each line using image SXM software (version 1.84). As clearly seen in Fig. 7(a), the degree of the line width increase with RH becomes large depending on the hydrophilicity of the sample surface. Namely, on the hydrophilic sample (carboxyl-SAM: water contact angle of 53°), the fabricated line becomes wider than that fabricated on the hydrophobic sample (methyl-SAM: water contact angle of 96°). This tendency is most distinct under the high humidity condition of 70% RH, while the difference is very small under the low humidity condition of 10% RH. The origin of this phenomena is most certainly the size effect of the water meniscus formed at the tip-sample junction. It is known that the tip-anodized Si size is determined by meniscus size.[24,25] It has also been reported that, on a hydrophobic SAM sample, the anodized line width is almost independent of humidity,[26] while on a hydrophilic oxide surface it shows a strong humidity dependence due to the widely spreading water meniscus under high humidity.[3] It should be noted that, under the low humidity condition of 10% RH, the line width is independent of surface hydrophilicity/hydrophobicity. The patterning resolution down to 20 nm was attained regardless of the SAM type. It is probable that, at this low humidity value, the water meniscus size is primarily governed by the tip condition, that is, radius and surface hydrophobicity. We will discuss later on this hydrophobic tip effect. These humidity and surface wettability effects on the water meniscus are schematically illustrated in Figs. 8(a)-(c). The solid, dashed, and dotted lines drawn at the tip-sample junctions indicate water meniscus at 10%, 40%, and 70% RH, respectively. Besides the line width, the line height behavior

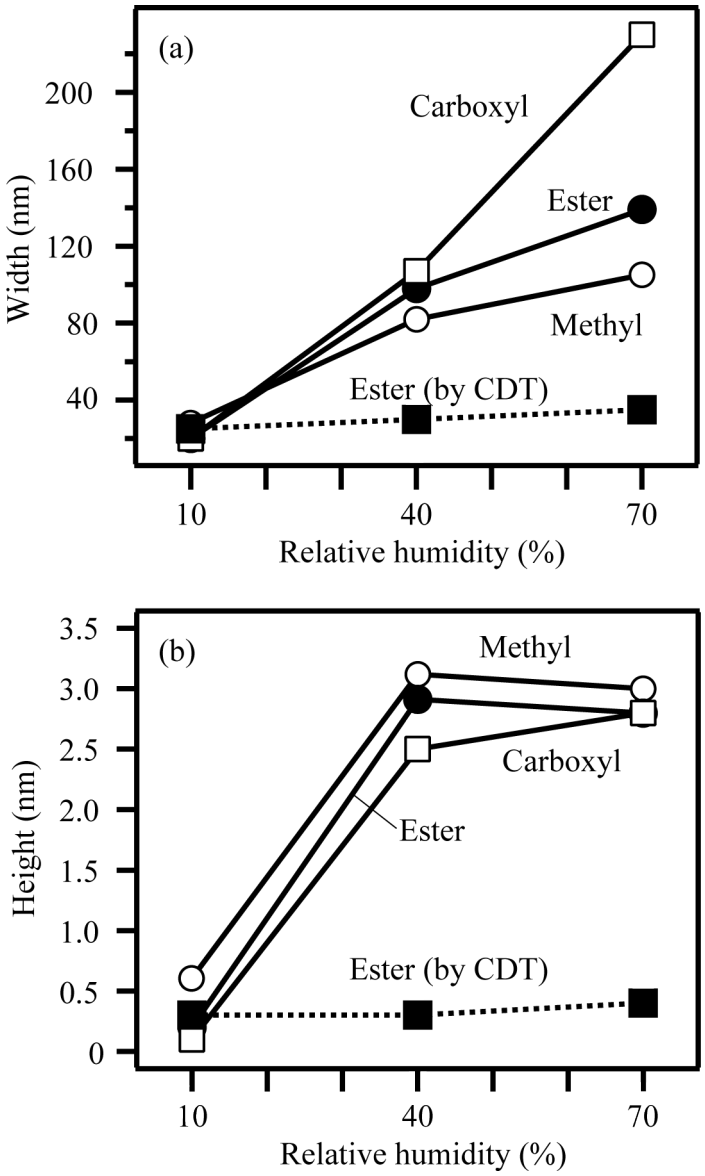

Fig. 7. Humidity and wettability effects on anodization patterning of the SAM samples. (a) Width and (b) height vs. RH. Solid and doted lines correspond to the results patterned by the Rh-tip and CDT, respectively.

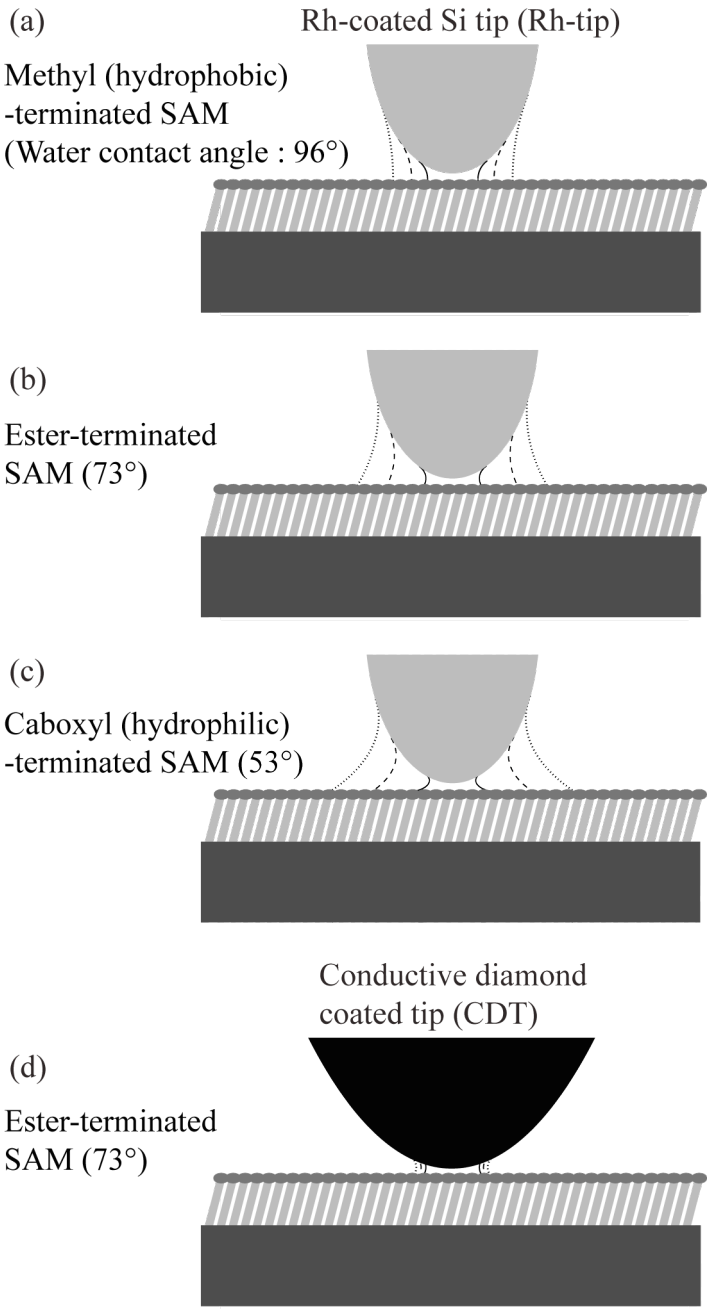

Fig. 8. Schematic illustration of the behavior of water meniscus dependent on humidity and wettability of sample and tip surfaces. Outermost lines drawn at the tip-sample junctions indicate water meniscuses under a high humidity condition, while innermost lines demonstrate water meniscuses under a low humidity condition. The junctions between a Rh-tip and (a) methyl-, (b) ester- or (c) carboxyl-SAM samples. (d) The junction between a CDT and an ester-SAM sample.

is summarized in Fig. 7(b) as well. The line height is less dependent on the surface wettability. Under all the humidity conditions, namely, 10, 40 and 70% RH, there are no significant difference in height between the lines fabricated on the methyl-, ester- and carboxyl-SAM samples. Furthermore, line heights fabricated at 40% and 70% RH are almost the same in the range of 2.5 - 3.0 nm, while those at 10% RH are smaller than 1.0 nm. These results can be explained based on the nature of anodization. In anodization at a constant voltage, the oxide thickness grown on a substrate surface first increases with time. However, it reaches a certain limit value determined by the voltage and the substrate material if anodization is prolonged for a sufficient period.[3,22,23,27,28)] Thus, we can conclude as follows. In the center area of each anodized line fabricated at 40% and 70%RH as shown in Figs. 6(b), 6(c), 6(e), 6(f), 6(h) and 6(i), the SAM was completely decomposed and the substrate Si was fully anodized so that the anodic Si oxide thickness in this area reached the limit value at a bias voltage of 10 V. We confirmed that a bias voltage of 10 V was enough to degrade the SAMs completely (not shown in this paper). On the other hand, in the case of the anodized lines fabricated at 10% RH as shown in Figs. 6(a), 6(d) and 6(g), anodization was not completed even at the center of each line, probably due to the shortage of adsorbed water which served as the source substance for electrochemical oxidation of SAM and Si.

Figure 9 shows the aspect ratios of the anodized lines as estimated from the results shown in Figs. 7(a) and 7(b). In the case of the Rh-tip patterning, the aspect ratios depend on RH and the surface wettability. The aspect ratios of the lines fabricated on the methyl-SAM sample, i.e., the most hydrophobic sample, are higher than those of the lines fabricated on the other SAMs which are relatively hydrophilic. In each SAM case, the aspect ratio becomes highest at 40% RH and decreases at 70%

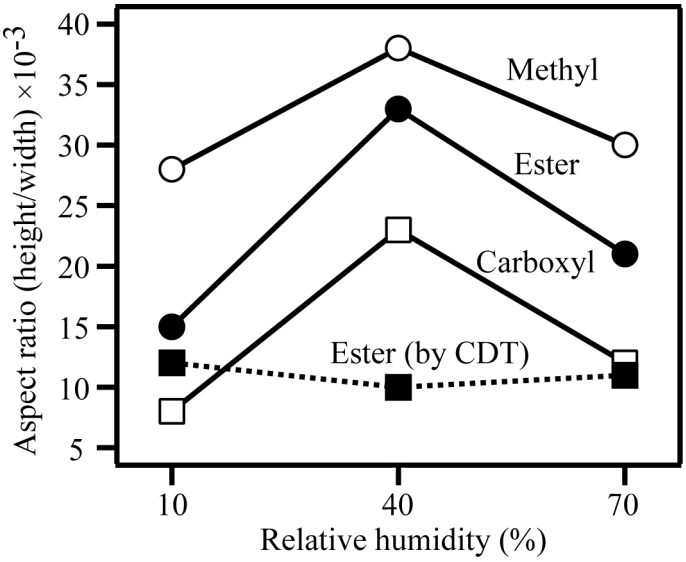

Fig. 9. Aspect ratios of the fabricated lines shown in Fig. 6 as functions of humidity. Solid and dotted lines correspond to the results patterned by the Rh-tip and CDT, respectively.

RH. Under the high humidity condition, the water meniscus formed at the tip-sample junction becomes fairly thick so that anodization takes place more widely in an area surrounding the tip contacting point. The combination of proper humidity and hydrophobic surface will help fabricate anodized lines of a higher aspect ratio.

We conducted the SPA patterning to know how much the Rh-tip was worn. Because the wear of a tip was a serious problem for all the SPM-based nanofabrication. Figure 10(a) shows the patterning result using the virgin Rh-tip at 10% RH. After SPA patterning at 10% RH was done, the patterning was performed at least ten times more to fabricate line patterns for other experiments. After that, SPA patterning was again performed to the different region at 10% RH. As a result, no distinct difference in the patterning line width was observed as shown in Fig. 10(b). We, therefore, found the tip-wear effect on pattern width did not take care in our experiments.

2.2.2. Topographical change in anodized lines by the conductive diamond tip

Here we discuss the results obtained using CDT and the ester-SAM sample. As shown in Figs. 6(j)-(l), there is no distinct humidity dependence of line width of the anodic patterns fabricated on the ester-SAM sample with a CDT. Similarly, it has been reported that fine oxide patterns were fabricated in ambient air with a carbon nanotube tip, which is expected to be relatively hydrophobic as well.[29)] As plotted in Fig. 7, the width of the anodized lines hardly changes with increasing RH from 10 % to 70 %. Accordingly, their aspect ratios do not change so much. In addition, the widths of the lines anodized by the CDT are comparable or even much smaller than those of the lines anodized by the Rh-tip. At 40% RH, the CDT line width is one forth of the Rh line width. The difference becomes much greater at 70% RH. The CDT line

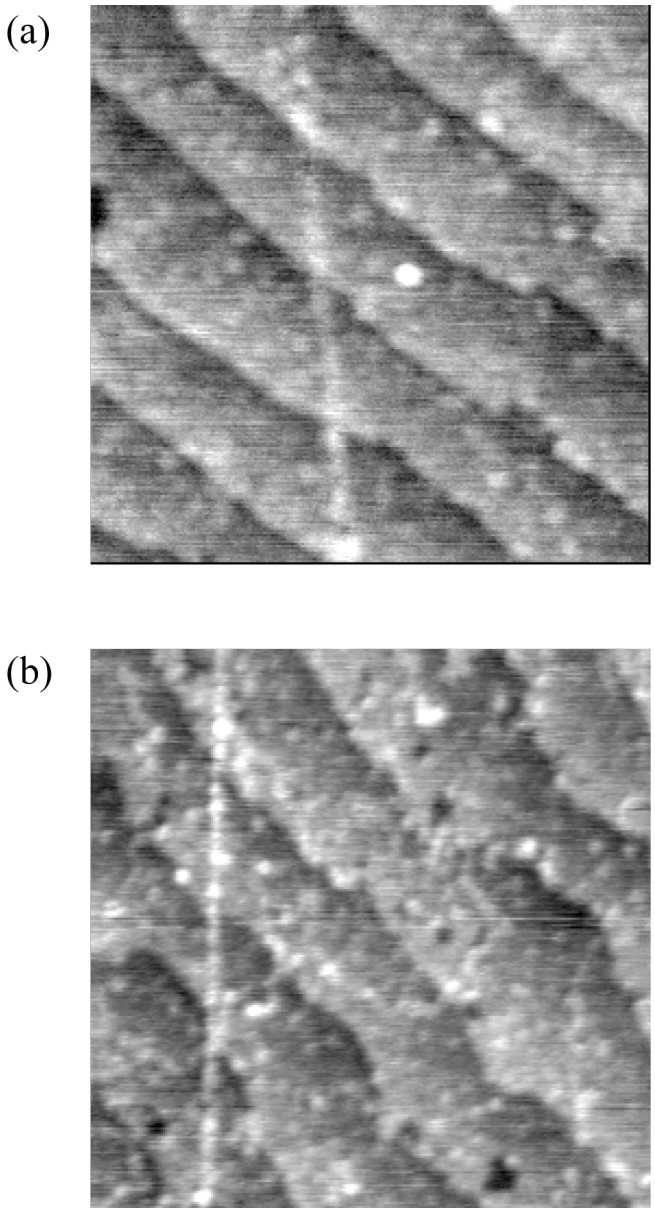

Fig. 10. Topographical images of ester-SAM sample with the line fabricated at 10% RH using (a) the virgin Rh-tip and (b) the same Rh-tip used at least several times before.

width is near one tenth of the Rh line width. These results are surprising considering the much larger tip radius of the CDT, i.e., 100 nm compared with that of the Rh-coated tip, i.e., 30 nm. There are two plausible explanations: the CDT surface has a hydrophobic nature[30] and hydrogen evolution ($2H + 2e^- \rightarrow H_2$) as a cathode reaction on the boron-doped diamond surface is slow.[31] It would be considered that the hydrophobic CDT possibly confines the adsorbed water meniscus in a restricted region under the tip as illustrated in Fig. 8(d). The slow hydrogen evolution rate at the cathode electrode, that is, the CDT surface in this case, might result in slow anode reactions at the sample surface, because the same number of electrons flows through the cathode and anode surfaces according to the basic principle of electrochemistry.

2.2.3. Force curve measurement

We performed force curve measurements on the ester-SAM sample surface in order to investigate the relative meniscus sizes of adsorbed water under the condition applying a tip-sample voltage of 10 V. A pull-off force was derived from each of the force curves. The pull-off force is considered to contain both the electrostatic force and the meniscus force. We assume that the electrostatic force is constant for the same AFM probe. Thus, the difference of the pull-off force is considered to indicate a difference of the meniscus force. The results are summarized in Fig. 11. Each value represents an average of ten pull-off forces measured under the same conditions. It should be noted that the absolute pull-off forces are very different between those obtained with the Rh-tip and with the CDT due to the large tip-radius difference, so we cannot compare their directly. We discuss only humidity dependencies of the pull-off forces. As shown in Fig. 11(a), the pull-off force increases with increasing RH, when measured by the Rh-tip. This pull-off force increase, therefore, most likely

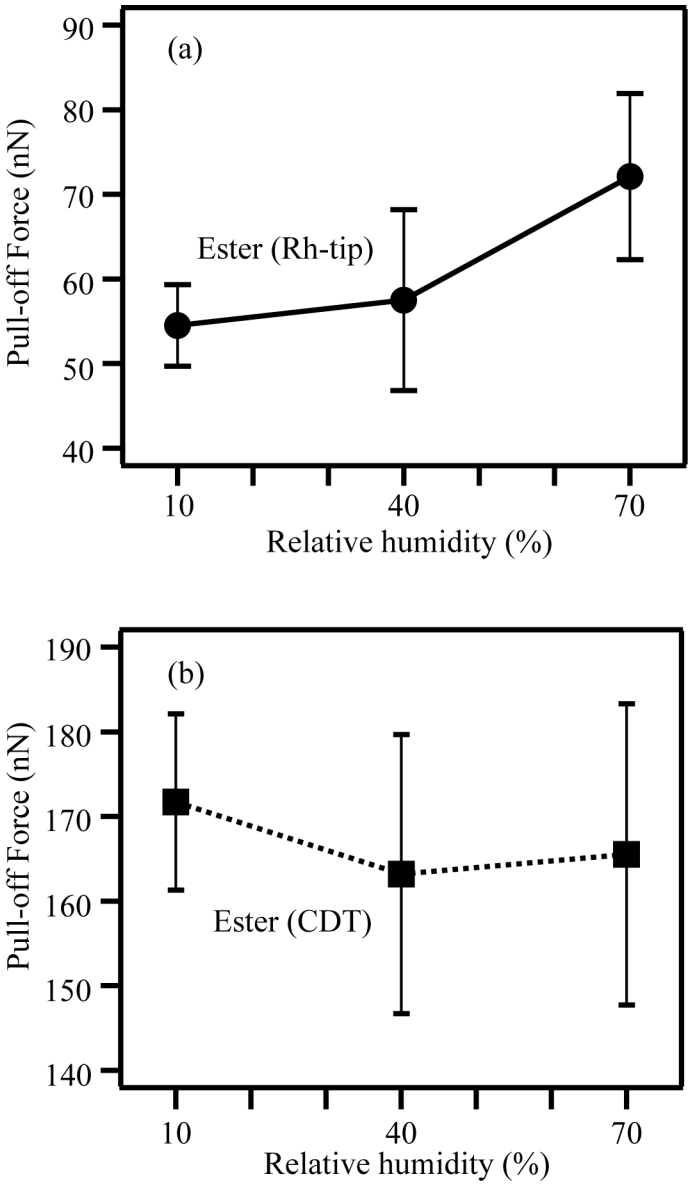

Fig. 11. Humidity dependence of pull-off force on the ester-SAM sample acquired by (a) the Rh-tip and (b) the CDT with a sample bias voltage of 10 V.

corresponds to an increase of meniscus size. This result agrees with the result of line widening under higher humidity as shown in Fig. 7(a). Several groups have reported similar force curve experiments with changing bias voltages.[32-34] On the other hand, in the case of the CDT as shown in Fig. 11(b), there is little change in pull-off force versus RH. This can be concluded to indicate no increase in meniscus size and agree with the pattern width results.

2.3. Summary

We have studied AFM-based scanning probe anodization of SAM-covered Si samples in terms of the effects of environmental humidity, surface wettability and probe-tip material on widths and heights of drawn lines. The AFM was operated in contact mode during the anodization patterning. We prepared three types of SAMs, that is, methyl-, ester- and carboxyl-terminated SAMs, of which the water contact angles were 96°, 73° and 53°, respectively, covalently immobilized on Si(111) surface through Si-C bonds. When the Rh-coated AFM tip was used for anodization, the patterned line width was markedly dependent on humidity and surface wettability. Namely, lower RH and/or more hydrophobic surface provided finer patterns. In contrast, when the CDT was used for anodization of the ester-SAM sample, the patterning was less humidity-dependent than with the Rh-tip. Furthermore, the CDT was found to enable drawing of lines with a comparable or even thinner width in spite of its tip radius of 100 nm being much larger than that of the Rh-tip, i.e., 30 nm. This is primary ascribable to hydrophobic nature of CDT which might confine the water meniscus in a restricted area as well as to a slow hydrogen evolution rate on the boron-doped diamond surface. Although, in this study, we were able to draw 20 nm

wide lines, the optimization of humidity and surface wettability of both tip and sample will lead to finer patterning.

References

1) H. Sugimura, in *Applied Scanning Probe Methods X, Biomimetics and Industrial Applications*, edited by B. Bhushan, H. Fuchs, and M. Tomitori, (Springer, 2008) p. 217.

2) H. Sugimura, T. Uchida, N. Kitamura, and H. Masuhara, Jpn. J. Appl. Phys. **32** (1993) L535.

3) H. Sugimura, T. Uchida, N. Kitamura, and H. Masuhara, J. Phys. Chem. **98** (1994) 4352.

4) E. S. Snow and P. M. Campbell, Appl. Phys. Lett. **64** (1994) 1932.

5) P. Avouris, T. Hertel, and R. Martel, Appl. Phys. Lett. **71** (1997) 285.

6) H. Sugimura and N. Makagiri, Langmuir **11** (1995) 3623.

7) C. Martin, G. Rius, X. Borrise, and F. P.-Murano, Nanotechnology **16** (2005) 1016.

8) S. M. Kim and H. Lee, J. Vac. Sci. Technol. B **21** (2003) 2398.

9) D. Wouters and U. S. Schubert, Angew. Chem. Int. Ed. **43** (2004) 2480.

10) M. R. Linford, P. Fenter, P. M. Eisenberger, and C. E. D. Chidsey, J. Am. Chem. Soc. **117** (1995) 3145.

11) P. Wagner, S. Nock, J. A. Spudich, W. D. Volkmuth, S. Chu, R. L. Cicero, C. P. Wade, M. R. Linford, and C. E. D. Chidsey, J. Struct. Biol. **119** (1997) 189.

12) M. M. Sung, G. J. Kluth, O. W. Yauw, and R. Maboudian, Langmuir **13** (1997) 6164.

13) N. Saito, S. Youda, K. Hayashi, H. Sugimura, and O. Takai, Surf. Sci. **532** (2003) 970.

14) M. Ara, H. Graaf, and H. Tada, Appl. Phys. Lett. **80** (2002) 2565.

15) B. Pignataro, A. Licciardello, S. Cataldo, G. Marletta, Mater. Sci. Eng. C **23** (2003) 7.

16) Y. Menglong, Z. Zhikun, L. Yaqing, and Z. Bailin, Nanotechnology **17** (2006) 330.

17) J. Han, H. Sano, Y. J. Kim, T. Ichill, K. Murase, and H. Sugimura (to be published).

18) H. Sugimura, A. Hozumi, T. Kameyama, and O. Takai, Surf. Interf. Anal. **34** (2002) 550.

19) H. Sugimura, H. Sano, K. -H. Lee, and K. Murase, Jpn. J. Appl. Phys. **45** (2006) 5456.

20) T. Strother, W. Cai. X. Zhao, R. J. Hamers, and L. M. Smith, J. Am. Chem. Soc. **122** (2000) 1205.

21) B. Fabre and F. Hauquier, J. Phys. Chem. B **110** (2006) 6848.

22) H. Sugimura, T. Hanji, K. Hayashi, and O. Takai, Ultramicroscopy **91** (2002) 221.

23) M. Yang, Z. Zhung, Y. Liu, and B. Zhang, J. Phys. Chem. B **110** (2006) 10365.

24) R. Garcia, M. Calleja, and H. Rohrer, J. Appl. Phys. **86** (1999) 1898.

25) C. R. Kinser, M. J. Schmitz, and M. C. Hersam, Nano letter **5** (2005) 91.

26) H. Sugimura, K. Okiguchi, and N. Nakagiri, Jpn. J. Appl. Phys. **35** (1996) 3749.

27) L. Young, in *Anodic Oxide Films* (Academic, New York, 1961).

28) T. Hurlen and E. Gulbandsen, Electrochim. Acta **39** (1994) 2169.

29) H. Dai, N. Franklin, and J. Han, Appl. Phys. Lett. **73** (1998) 1508.

30) M. J. Schmitz, C. R. Kinser, N. E. Cortes, and M. C. Hersam, Small **3** (2007) 2053.

31) H. B. Martin, A. Argoitia, U. Landau, A. B. Anderson, and J. C. Angus, J. Electrochem. Soc. **143** (1996) L133.

32) S. F. Lyuksyutov, P. B. Paramonov, I. Dolog, and R. M. Ralich, Nanotechnology **14** (2003) 716.

33) C. Martin, F. P. Murano, and J. A. Dagata, IEEE (2003) 781.

34) S. Hoeppener, J. H. K. van Schaik, and U. S. Schubert, Adv. Funct. Mater. **16** (2006) 76.

3. KFM and SCM application for SAM-covered Si samples patterned by SPM

Nanoscale patterning of Si substrates covered with SAMs has attracted much attention, because a wide variety of functionalities can be provided on the Si substrate with nano-scale spatial resolution by using the patterned SAMs as etching masks and chemical templates.[1-3] SPM is a powerful means for nanopatterning and observation of SAM/Si samples.[4-10] Characterization of patterned SAM/Si samples based on SPM has been mainly conducted so far by acquiring topographic and frictional images. Electrical characterization of the nanopatterned samples by other SPM techniques was rarely applied.

Both KFM and SCM are well-known as valuable techniques for the electrical characterization of semiconductor materials and devices. For example, local charge trapping into a nitride/oxide bilayer - Si sample and its imaging were demonstrated by the use of SCM.[11] Si p-n junctions were clearly imaged by KFM[12] and SCM.[13] Thus, the characterization by these two SPMs is of special interest for SAM covered Si samples. Indeed, Nakagiri *et al*. have reported SCM and KFM contrasts of Si substrates with p-, n-, and n^+-type regions covered with organosilane SAMs.[14] KFM has been proved to be applicable for the imaging of nano-scale patterns on a SAM/Si sample surface fabricated by scanning probe anodization.[15] However, SCM imaging of such a sample has not been conducted yet. Since KFM provides information of the surface and SCM does that of the insulator-Si interface, it will be more informative when these SPMs are used complementary.

In this paper, we report on patterning and characterization of Si substrate covered with an organosilane SAM by SPM. The samples were locally modified by a current-injection AFM with a conductive probe. The modified surfaces were imaged by KFM and SCM.

3.1. Experimental procedure

Two types of Si samples were used in this study. One was an n-type Si substrate (resistivity of 4 - 6 Ω cm) with phosphorous doped density of 1×10^{15} cm^{-3}. The other was a p-type Si substrate with boron doped density of 2×10^{16} cm^{-3}. This p-type Si substrate was prepared by ion-implantation into the n-type Si substrate mentioned above. The samples were cleaned by sonication with alcohol for 10 min and with pure water for 10 min, and dried with N_2 gas flow. The removal of organic contamination on the substrates was carried out by VUV light irradiation in air. A clean oxide layer of ca. 2 nm thick was formed on the substrate surfaces. An octadecylsilyl SAM (ODS-SAM) was then formed on the VUV-cleaned samples by a vapor phase method. Details of the cleaning and SAM formation methods were described elsewhere.[16] The water contact angle of the ODS-SAM surface was about 103°.

The ODS-SAM/SiO_2/Si samples were modified by applying a sample bias in the range of 1 - 9 V using an SPM with a Pt-Ir coated Si probe (force constant of 2.2 N/m, resonance frequency of 74 kHz). The polarity of the bias was set as the sample being positive. As schematically illustrated in Fig. 1, by applying a bias voltage, nine areas of 0.8×0.8 μm^2 were scanned at a scan rate of 0.5 μm/s in air (24 ˚C, 35% RH) on each of the samples. The probe-scanned samples were imaged by KFM, SCM and, LFM modes of the same AFM used for the surface modification. The KFM measurements were conducted using a Rh-coated cantilever with a resonance frequency of 27 kHz and a force constant of 1.6 N/m at a scanning speed of 0.3 Hz. The LFM measurements were performed by the same cantilever used for the KFM measurements. A Pt-Ir coated cantilever of a resonance frequency of 22 kHz and a force constant of 2.2 N/m was used for the SCM measurements with a scanning speed

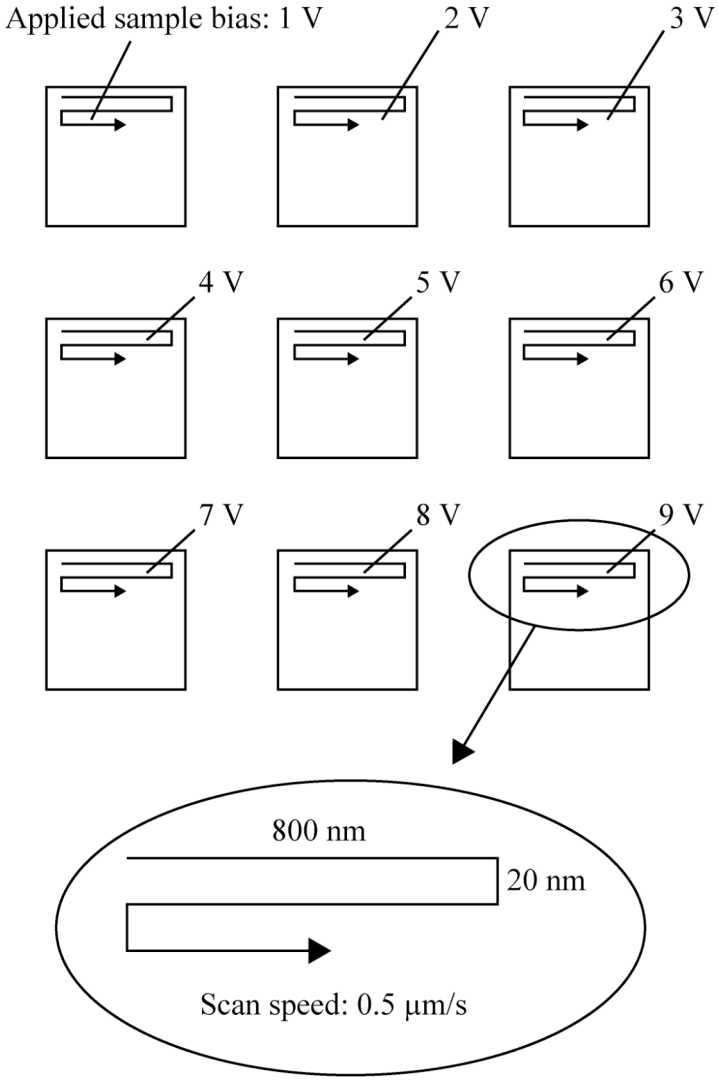

Fig. 1. Schematic diagram of pattern drawing. Nine square (0.8×0.8 μm^2 size) were drawn on each of the ODS-SAM coated p- and n-type Si samples with applying a bias voltage in the range of 1 - 9 V at a probe scan rate of 0.5 μm/s.

of 1 Hz, which is developed by Seiko Instruments Inc. based on the Scanning nonlinear dielectric microscopy. [14,17] An AC modulation (5 kHz, 2 V) was applied to the sample. The KFM and SCM measurements were carried out about 6 hours and 20 hours later respectively, after patterning of the nine squares. As for the measurement environments, KFM was used in an N_2 purged atmosphere, and the LFM and SCM measurements were conduced in vacuum, in order to minimize adsorbed water effects.[18]

3.2. Results and discussion

3.2.1. KFM, LFM, and SCM characterization in p-type Si substrates covered with a SAM

Figure 2 shows KFM, LFM and SCM images of the modified ODS-SAM/SiO_2/p-Si sample. As clearly seen in the KFM image [Fig. 2(a)], nine square patterns show lower surface potentials compared with the unmodified sample area. The surface potential becomes lower when scanned with the applied bias between 1 and 4 V. However, it turns to increase in the bias range more than 4 V. In contrast, as shown in Fig. 2(b), the squares drawn at 7, 8, and 9 V can be recognized as regions more frictional than the unmodified area in the LFM image. This means that some chemical changes were induced on the sample surface at these bias voltages. As reported previously, when a Si sample covered with an ODS-SAM was scanned by a conductive AFM probe with a positive sample bias, the ODS-SAM was degraded and the underlying Si substrate was anodized due to electrochemical oxidation reactions induced in the adsorbed water column formed at the probe-sample junction.[19] The degradation degree increased with the bias voltage. Consequently, the underlying oxide surface was exposed to some extent according to the degradation degree of the

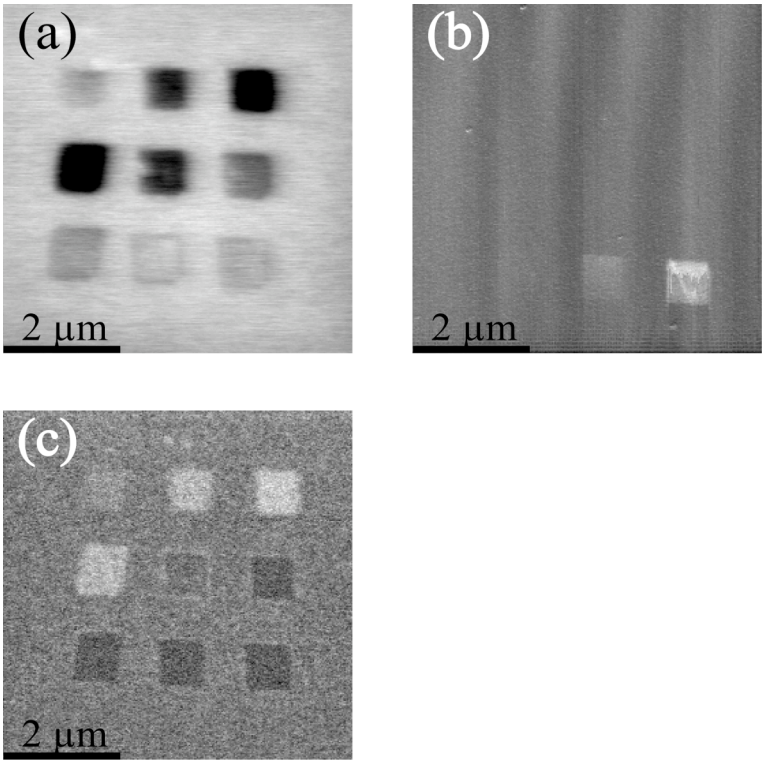

Fig. 2. SPM images of the modified ODS-SAM/SiO_2/p-Si sample. (a) KFM image acquired in N_2, (b) LFM image acquired in vacuum, and (c) SCM image acquired in vacuum.

ODS-SAM. The relatively higher surface potentials of the square regions fabricated at 7 - 9 V than the regions scanned with lower sample biases are ascribed to the degradation of the ODS-SAM, since, when the ODS-SAM was completely removed, the sample surface showed a higher surface potential than that of the undegraded ODS-SAM.[20)]

In the low bias range of 1 - 4 V, the origin of the surface potential changes cannot be ascribed to the degradation of the ODS-SAM. At this range, the bias voltage is considered to be too low to induce electrochemical oxidation of saturated hydrocarbon molecules. Charge trapping at both ODS-SAM and SiO_2 layer in addition to charge deposition in the ODS-SAM surface is plausible to explain the surface potential change at the low bias voltages. Richter *et al*. have characterized I/V features of alkyl/SiO_2 and SiO_2/Si interfaces using Au/alkylsilane/SiO_2/Si samples and confirmed that charge trapping and detrapping proceeded at both the interfaces when a bias voltage less than 2 V was applied between the Au and Si layers.[21)] Besides the interfacial charge trapping, charges are known to be deposited onto an insulator surface from an electrified SPM tip.[22)] In the intermediate bias range of 5 - 6 V, the principal origin of the surface potential change is considered to be charge trapping and deposition as well. Although a faint chemical change may be induced on the ODS-SAM surface, its degree is very slight since there are no apparent contrasts in the LFM image. Consequently, chemical effects on the surface potential are assumed to be negligible. It should be noted that the threshold voltages are not distinct and not definitely constant. Those depend on surface modification conditions such as humidity, qualities of SAM and oxide, probe scan rate, and so on.

Figure 2(c) shows an SCM image acquired by applying a DC offset of 1 V and an AC modulation of 2 V at a frequency of 5 kHz. The contrast in the SCM image

seems to have the relation with contrast variation in the KFM image. The SCM signal of the square patterns fabricated at 1 - 4 V are higher than that of the surrounding unmodified area, while those of the squares fabricated at 5 - 9 V are lower than the unmodified area.

On each of the modified square regions and the unmodified area, dC/dV-V curves were acquired with a 2 V-AC modulation of 5 kHz as shown in Fig. 3. The peak positions of the dC/dV-V curves obtained on the regions patterned with a bias of 1 - 4 V slightly shift to the negative direction compared with the peak of the unmodified area, while the curve peaks acquired on the regions modified at a bias of 5 - 9 V are located on the positions distinctly more positive than that of the unmodified area. These peak shifts in the dC/dV-V curves are consistent with the SCM image results.

As schematically illustrated in Fig. 4, the charge trapping behavior is assumed to depend on the applied sample bias voltage. We, here, describe the charge trap phenomenon with respect to probe tip bias in order to readily understand this phenomenon. When a negative tip bias, namely, a positive sample bias as similarly to our study, is applied to the ODS-SAM surface, the valence band of the substrate p-Si bends upward and the majority carriers, namely, holes in this case, are accumulated near the semiconductor surface, as well-known in metal-oxide-semiconductor (MOS) devices.[23] As shown in Fig. 4(b), when a low negative tip bias of 1 - 4 V is applied, the upward band bending is not serious, thus, an amount of the accumulated positive charge is too small to affect charge trapping behavior. Negative charges are injected in both the ODS-SAM and SiO_2 layer from the tip. However, as shown in Fig. 4(c), at a higher sample bias voltage, the trapped charge in the SiO_2 layer is replaced by positive charges from the p-Si substrate, due to the more negative tip bias which

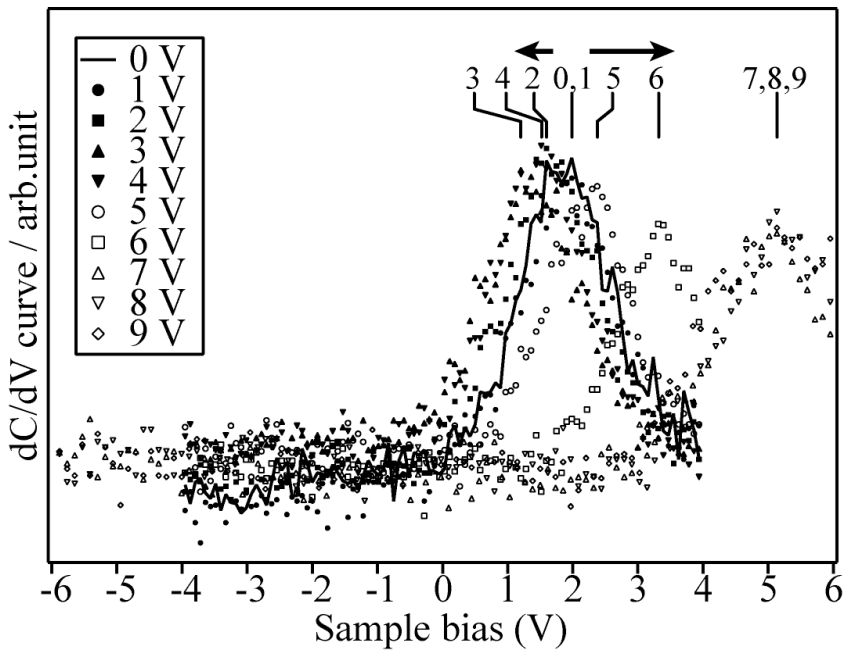

Fig. 3. dC/dV-V curves acquired at the unmodified area and the probe-scanned regions on the ODS-SAM/SiO_2/p-Si sample.

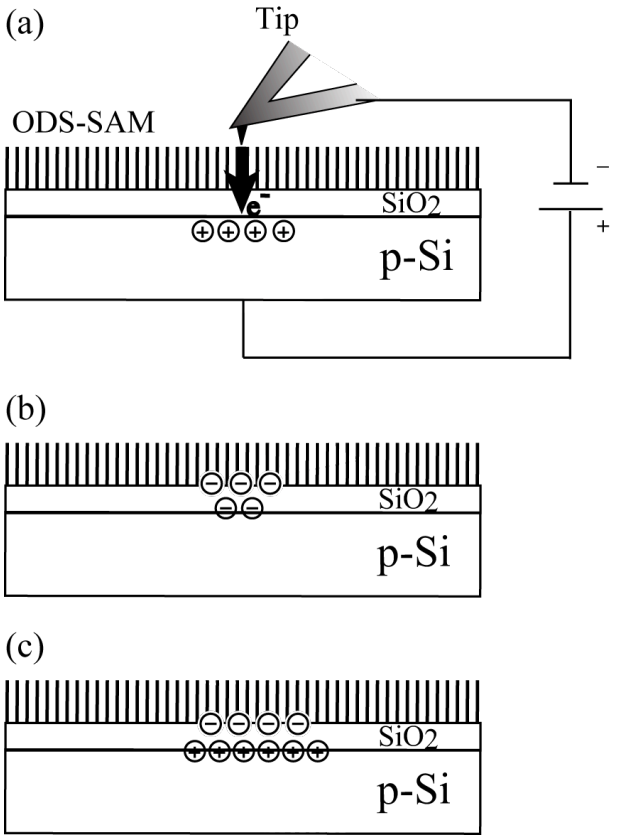

Fig. 4. Schematic diagram for charge trapping in both the ODS-SAM/SiO_2 interface and SiO_2 layer in case of p-Si sample. (a) Local charging using an AFM probe, (b) negative charge trapping at a low bias voltage, and (c) positive charge trapping from the p-Si substrate at a high bias voltage.

generates a higher band vending and promotes to accumulate positive charges from the p-Si substrate to charge trapping sites in the SiO_2 layer. Similar results, that is, positive charge trapping at the SiO_2/Si interface of a MOS structure by a negative gate bias, have been reported.[24] Hence this positive charge trapping behavior can more clearly explain the change in the contrast of the surface potential of the square patterns in Fig. 2(a) and in the shift of the dC/dV-V curve in Fig. 3, from the region of an applied bias voltage of 5 V.

3.2.2. KFM, LFM, and SCM characterization in n-type Si substrates covered with a SAM

Next, we show results on the ODS-SAM/SiO_2/n-Si sample. Figure 5 shows SPM images of the modified sample acquired by (a) KFM, (b) LFM, and (c) SCM modes, respectively. The results are similar to those of the p-type Si sample as shown in Fig. 2 except for the SCM result [Fig. 5(c)] which is acquired by applying a bias of a DC offset of - 2 V and an AC modulation of 2 V at a frequency of 5 kHz. All the square regions show higher SCM signals than the surrounding unmodified area, indicating that charge trapping behavior is different from the p-Si sample.

As shown in Fig. 6, the peak position of dC/dV-V curves shift toward negative direction with respect to the peak position of the dC/dV-V curve acquired on the surrounding unmodified area. This negative peak shift means negative charge trap in both the ODS-SAM/SiO_2 interface and SiO_2 layer.

As shown in Fig. 7, in the case of n-Si, the upward band bending induced by a negative tip bias results in its carriers, i.e., electrons, being depleted from near the semiconductor surface.[23] The electrons injected from the tip are trapped at the trap

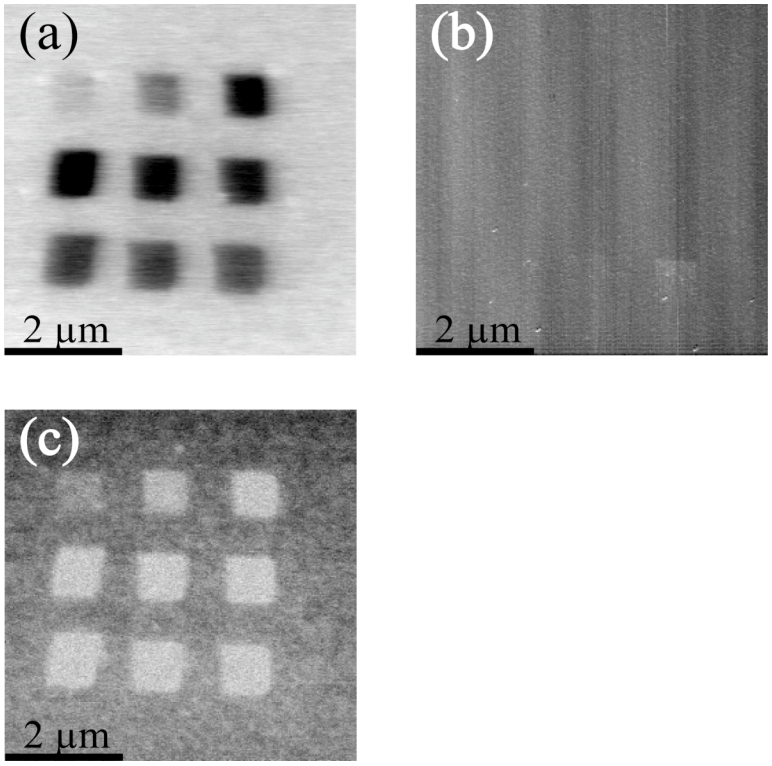

Fig. 5. SPM images of the modified ODS-SAM/SiO_2/n-Si sample. (a) KFM image acquired in N_2, (b) LFM image acquired in vacuum, and (c) SCM image acquired in vacuum.

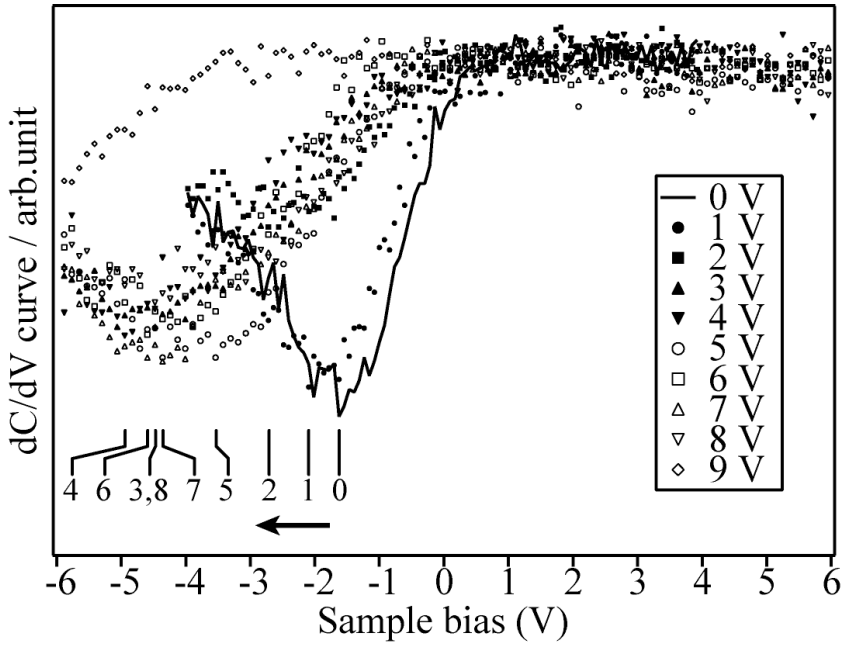

Fig. 6. dC/dV-V curves acquired at the unmodified area and the probe-scanned regions on the ODS-SAM/SiO_2/n-Si sample.

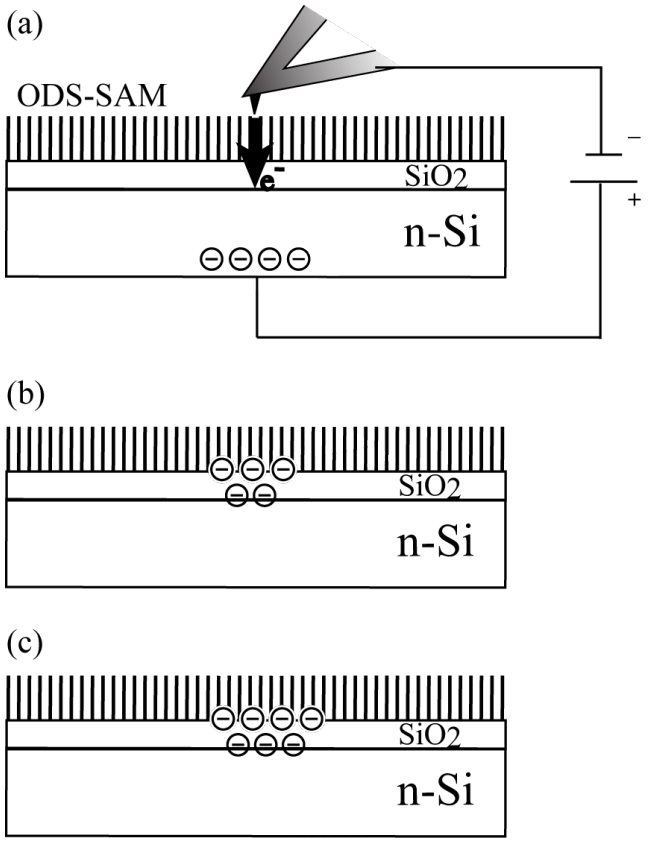

Fig. 7. Schematic diagram for charge trapping in both the ODS-SAM/SiO_2 interface and SiO_2 layer in case of n-Si sample. (a) Local charging using an AFM probe, (b) negative charge trapping at a low bias voltage, and (c) more densely trapped negative charge at a high bias voltage.

sites and not replaced with positive charges because there are few carriers in the depletion layer.

3.3. Summary

We have studied on the localized charging into the ODS-SAM/SiO_2/Si (p- and n-type) samples by the use of AFM. A positive sample bias was applied between a conductive AFM probe and the substrate Si. The modified samples were characterized KFM, SCM and LFM. At the bias range of 7 - 9 V, the ODS-SAM was degraded due to electrochemical reactions with adsorbed water as confirmed by the LFM images indicating that the regions scanned with a sample bias in this range had more frictional than the unmodified ODS-SAM area. There were no apparent LFM contrasts on the regions scanned with a bias voltage less than 7 V, while the regions showed distinct KFM and SCM contrasts. In this low bias range, particularly less than 5 V, the surface modification mechanism was ascribed not to the degradation of the ODS-SAM but to the charge trapping and deposition in the ODS-SAM/SiO_2 interface and SiO_2 layer. The SCM observation revealed that the charge trapping behavior was different depending on the carrier types of the Si substrates. When p-type Si was used as the substrate the polarity of the trapped charge was inverted from negative to positive with the increase in the bias voltage for current injection, while negative charge trapping was observed for the ODS-SAM/SiO_2/n-Si all the bias range for the sample. This carrier type dependency on charge trapping could not be elucidated by the KFM observation alone. Therefore, the complimentary use of KFM and SCM is crucial for characterization of organic monolayer - semiconductor interfaces.

References

1) W. J. Dressick and J. M. Calvert, Jpn. J. Appl. Phys. **32** (1993) 5829.

2) X.-M. Li, J. Huskens and D. N. Reinhoudt, J. Mater. Chem. **14** (2004) 2954.

3) H. Sugimura, Int. J. Nanotech. **2** (2005) 314.

4) C. R. K. Marrian, F. K. Perkins, S. L. Brandow, T. S. Koloski, E. A. Dobisz and J. M. Calvert, Appl. Phys. Lett. **64** (1994) 390.

5) F. K. Perkins, E. A. Dobisz, S. L. Brandow, T. S. Koloski, J. M. Calvert, K. W. Rhee, J. E. Kosakowski and C. R. K. Marrian, J. Vac. Sci. Technol. B **12** (1994) 3725.

6) H. Sugimura and N. Nakagiri, Langmuir **11** (1995) 3623.

7) H. Sugimura, K. Okiguchi, N. Nakagiri and M. Miyashita, J. Vac. Sci. Technol. B **14** (1996) 4140.

8) H. Sugimura and N. Nakagiri, J. Am. Chem. Soc. **119** (1997) 9226.

9) R. Maoz, S. R Cohen and J. Sagiv, Adv. Mater. **11** (1999) 55.

10) Y. Cai and B. M. Ocko, J. Am. Chem. Soc. **127** (2005) 16287.

11) R. C. Barrett and C. F. Quate, J. Appl. Phys. **70** (1991) 2725.

12) A. Kikukawa, S. Hosaka and R. Imura, Appl. Phys. Lett. **66** (1995) 3510.

13) T. Yamamoto, Y. Suzuki, M. Miyashita, H. Sugimura and N. Nalagiri, Jpn. J. Appl. Phys. **36** (1997) 1922.

14) N. Nakagiri, H. Sugimura, Y. Ishida, K. Hayashi and O. Takai, Surf. Sci. **532** (2003) 999.

15) H. Sugimura, T. Hanji, K. Hayashi and O. Takai, Adv. Mater. **14** (2002) 524.

16) H. Sugimura, A. Hozumi, T. Kameyama and O. Takai, Surf. Interf. Anal. **34** (2002) 550.

17) Y. Cho, S. Kazuta and K. Matsuura, Appl. Phys. Lett. **75** (1999) 2833.

18) H. Sugimura, Y. Ishida, K. Hayashi and O. Takai, Appl. Phys. Lett. **80** (2002) 1459.

19) H. Sugimura, T. Hanji, K. Hayashi and O. Takai, Ultramicroscopy **91** (2002) 221.

20) H. Sugimura, K. Hayashi, N. Saito, N. Nakagiri and O. Takai, Appl. Surf. Sci. **188** (2002) 403.

21) C. A. Richter, C. A. Hacker, L. J. Richter, O. A. Kirillov, J. S. Suehle and E. M. Vogel, Solid-State Electron. **50** (2006) 1088.

22) Y. Fukano, T. Uchihashi, T. Okusano, A. Cyayahara, Y. Sugawara, Y. Yamanishi, T. Oasa and S. Morita, Jpn. J. Appl. Phys. **33** (1993) 379.

23) S. M. Sze, *Physics of Semiconductor Devices* (Wiley, New York, 1981) 2nd ed., p. 365.

24) T. Brozek and C. R. Viswanathan, Appl. Phys. Lett. **68** (1996) 1826.

4. Charge trapping behavior of SAM/Si systems with and without an interfacial oxide layer by SPM

Much attention has been paid to organic molecular films including monolayers as active and passive elements of electronic devices.[1-3] In particular, SAMs are of primary importance, since such films are applicable as an insulating layer of field-effect transistors (FETs) and metal-insulator-metal diodes,[4-11] a semiconducting layer in organic FETs,[12,13] diffusion barrier coatings for Cu metallization,[14,15] photodiodes,[16] charge storage layers,[17-19] reduction of metal-silicon contact resistance[20] and chemical FET sensors.[21-23] Furthermore, when an organosilane SAM is inserted between the gate oxide/organic semiconductor interface of an organic FET, its mobility and threshold voltage are dependant on the SAM.[24-27] This is considered to be due the modified surface potential of the gate oxide originating from the dipole moment of the silane molecules in the SAM[28] and due to improved crystallinity of the organic semiconductor film formed on a specific type of SAM surface.[26,27] Among various types of such organic monolayers, SAMs formed on Si substrates are of particular interest from the viewpoint of their potential as an insulating layer in Si microelectronics. There are two major forms of SAM on Si. One is an organosilane SAM formed on oxide-covered Si substrates through silane-coupling chemistry,[29,30] and the other is a SAM covalently attached to Si through Si-C or Si-O-C bonds and so forth.[31,32]

Understanding the electric properties of SAMs on Si is of primary importance in order to develop SAM-based microdevices. Such properties have been measured so far by fabricating metal/SAM/Si samples in which a gate metal electrode was evaporated or sputtered on a SAM-covered Si substrate.[4-6,9] However, with the advent of smaller devices, a new instrument is required to effectively characterize and

investigate SAMs in a smaller area. As an alternative tool, SPM is a powerful technique. For example, current-sensing atomic force microscopy (CS-AFM) has been successfully applied in order to measure local conductivities of SAMs formed on metal and Si surfaces.[33-35] Several types of SPM-based methods other than CS-AFM have been developed in order to characterize electrical properties. KFM and SCM are attractive techniques for the characterization of semiconductor material surfaces and semiconductor/insulator interfaces.[36-41] Furthermore, SPM can be used as a nano-tool for locally stimulating or pertubating a sample surface. The combination of the investigation and modification functions of SPM might be useful for studies of SAM/Si interfaces.

Here, we report on the SPM-characterization results for two types of SAM samples formed on Si substrates, that is, an alkylsilane SAM formed on an oxide-covered Si substrate and an alkyl SAM formed directly on a Si substrate without surface oxide. Into these SAM samples, current was locally injected from a conductive AFM probe tip at various substrate bias voltages. The current-injected samples were characterized by KFM and SCM in addition to topographic imaging.

4.1. Experimental procedure

Two types of SAM-covered samples were prepared. One was a hexadecyl SAM (HD-SAM) formed on a n-type (resistivity of 1 - 10 Ω cm) Si(111) substrate with an hydrogen-terminated Si surface.[42] The other was ODS-SAM grafted on the same Si substrate with a native oxide layer of approximately 2 nm thick.[30] , as described in chapter 3. Water contact angles and ellipsometric thicknesses of the HD-SAM and the ODS-SAM were approximately 108° and 103°, and 2.3 and 1.5 nm,

respectively. The absence of oxide at the HD-SAM/Si interface was confirmed by X-ray photoelectron spectroscopy.

SPM experiments were conducted using a commercial SPM. Current was locally injected into each sample surface from a Pt/Ir-coated Si probe tip. The polarity of the bias was set with the Si substrate being positive. A modification bias voltage (V_m) in the range of 1 - 9 V was applied to the SAM-covered samples in humidity-controlled air (24 ˚C, 40% RH). The probe was scanned in an 800 nm × 800 nm square area at a rate of 0.5 μm/s, as illustrated in chapter 3. KFM measurements of the current-injected samples were conducted using a Rh-coated probe tip with 2 V AC at a frequency of 25 kHz. SCM measurements were also done using the Pt/Ir-coated probe tip with 2 V AC at the frequency of 5 kHz and DC offset of 0 V (for the HD-SAM sample) or -2 V (for the ODS-SAM sample). These KFM and SCM measurements were carried out in a N_2 purged atmosphere and in vacuum, respectively, in order to minimize adsorbed water effects.[43)]

4.2. Results and discussion

4.2.1. SPA of both the SAM/Si systems

Figure 1 shows topographic, KFM, and SCM images of the HD-SAM sample and the ODS-SAM sample on each of which nine square regions had been scanned with a bias voltage. The square regions scanned with V_m = 6 - 9 V on the HD-SAM sample were protruded as shown in Fig. 1(b), while, on the ODS-SAM sample, the square region scanned with V_m = 7 - 9 V is observable as shown in Fig. 1(f). These topographic changes in the HD-SAM and ODS-SAM samples are ascribable to anodization of substrate Si. When a proper bias is applied to the SPM probe/sample junction, the organic monolayer is degraded and the substrate Si is anodized.

Consequently, a protruded pattern is formed due to the volume expansion accompanied with oxidation of Si to SiO_x.[44,45] The difference in the threshold voltage between the HD-SAM and ODS-SAM samples is considered to be due to the difference in the amount of current flow between the tip and the substrate, which can be superior to the sample of the absence of a native oxide layer,[46] and the difference in thickness. As schematically illustrated in Fig. 1(a), on the HD-SAM sample, there is only an alkyl layer 2.3 nm thick. However, as illustrated in Fig. 1(e), there are two insulating layers on the ODS-SAM sample. Their total thickness is 3.5 nm (ODS-SAM; 1.5 nm, oxide; 2.0 nm). Thus, a higher bias voltage is needed for the ODS-SAM sample in order to generate a sufficiently strong electric field promoting degradation of the organic monolayer and anodization of Si.

4.2.2. KFM measurement of the SAM/Si systems

In the case of the HD-SAM sample, four square patterns fabricated at V_m = 6 - 9 V appear dark (lower surface potentials with respect to the surrounding area) in the KFM image of Fig. 1(c). These square regions correspond to the regions with apparent topographic change as shown in Fig. 1(b). The origin of the surface potential changes is ascribable to degradation of the HD-SAM and anodization of the substrate Si. In contrast, in the case of the ODS-SAM sample, all the nine square patterns fabricated at V_m = 1 - 9 V are clearly seen in the KFM image of Fig. 1(g), in spite of the fact that topographic changes are not apparent at the regions scanned with V_m = 1 - 6 V. These results indicate that the changes in surface potential at the regions scanned with V_m = 1 - 6 V do not originate from SAM degradation and Si anodization, unlike the case of the HD-SAM sample.

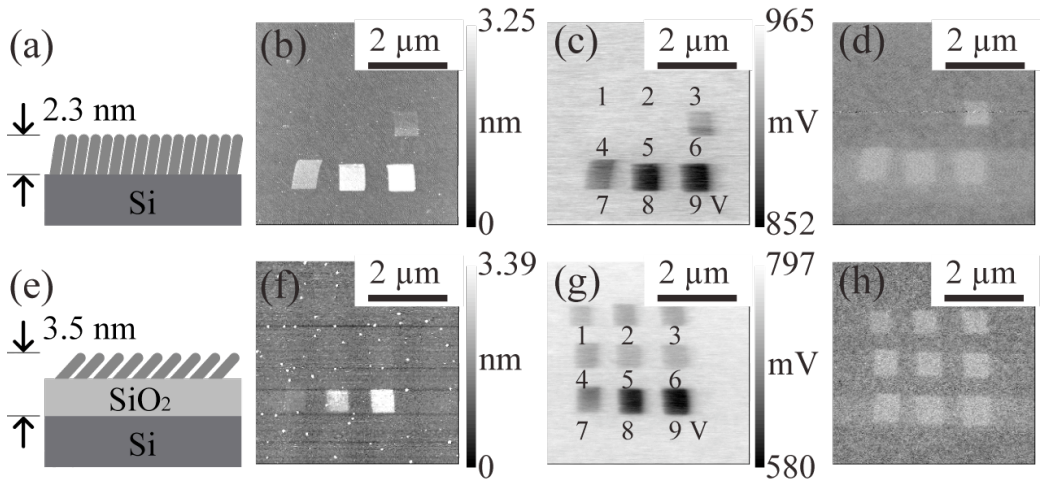

Fig. 1. Schematic illustrations of the HD-SAM sample and the ODS-SAM sample, and experimental results. (a) Cross section of the HD-SAM sample. (b) Topographic, (c) KFM and (d) SCM images (2 V AC at the frequency of 5 kHz and DC offset of 0 V) of the HD-SAM sample with nine square regions scanned at a bias voltage. (e) Cross section of the ODS-SAM sample. (f) Topographic, (g) KFM and (h) SCM images (2 V AC at the frequency of 5 kHz and DC offset of -2 V) of the ODS-SAM sample with nine square regions scanned at a bias voltage.

These changes of surface potential are summarized as functions of V_m in Fig. 2. The surface potentials at the regions scanned with V_m = 1 - 6 V on the ODS-SAM sample show almost constant values in the range of -40 ~ -60 mV. The origin of these surface potential drops is most likely negative charge trapping at an oxide layer or Si/SiO_2 interface, since there are no changes in the ODS-SAM and the substrate Si as clearly demonstrated by the corresponding topographic image [Fig. 1(b)]. It has been reported that such charge trapping in an insulating layer caused a surface potential shift, as confirmed by SPM.[36,41,47] Charge trapping behavior at the Si/SiO_2 interface is known to be dependent on the oxide layer thickness.[48,49] According to reported results, when the thickness of an oxide used as an insulating layer of FETs is below approximately 4 nm, the interface between oxide and Si plays important roles in charge trapping. However, the amount of trapped charge does not show a significant dependence on the bias voltage. Thus, in our case, it can be understood that the surface potential values of the regions modified with V_m = 1 - 6 V are almost constant, because the oxide thickness of this sample was about 2 nm. In the regions scanned with V_m = 7 - 9 V, the surface potential decreased more than that of the regions scanned with V_m = 1 - 6 V. In these bias regions, there are three plausible mechanisms for the surface potential drop: the charge trapping at the oxide and Si/oxide interface; the growth of anodic oxide; and the chemical conversion of the outermost SAM surface. It is doubtless that all these three mechanisms contribute to the surface potential drop. However, their contribution degrees are supposed to be unequal. From V_m = 7 - 8 V, the potential drop is abrupt as shown in Fig. 2. This is mainly ascribed to oxidation of the outmost surface of the ODS-SAM. At the initial stage of anodization of the ODS-SAM sample, methyl groups terminating its surface are oxidized to functional groups containing oxygen atoms, e.g., carboxyl groups.[50,51]

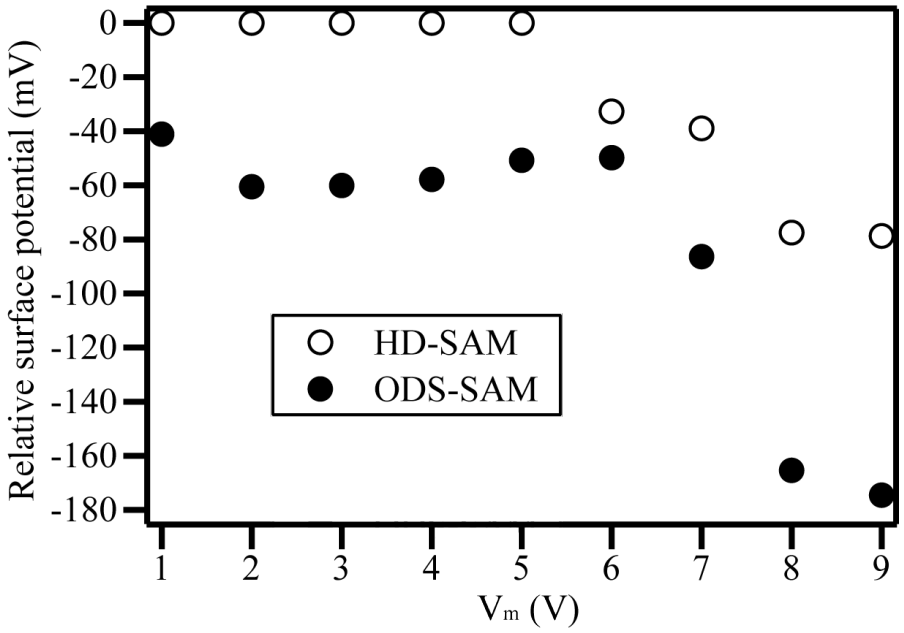

Fig. 2. Relative surface potentials of the square regions on the HD-SAM sample and the ODS-SAM sample with respect to the corresponding un-scanned region.

The presence of carboxyl groups on an alkyl SAM surface shifts its surface potential to more negative.[50] It is certain that the ODS-SAM was decomposed and removed from the modified regions at these V_m = 7 - 8 V values.[44] Accordingly, the chemical properties of these regions are considered to be similar. Thus, there was a little change in surface potential due to the chemical origin. The surface potential drops at the region oxidized with V_m = 7 - 8 V are mainly governed by charge trapping with an increased thickness, probably thicker than 4 nm, due to anodization. The amounts of trapped charges would be increased so that the surface potentials became more negative compared with the regions modified with V_m = 1 - 6 V where not anodized. In the case of the HD-SAM sample, there was no surface potential drop at the regions scanned with V_m = 1 - 5 V as described above. Although chemical changes of the HD-SAM and charge deposition on the SAM, that is, an insulator, might have occurred,[52,53] such phenomena seemed to be negligible in our case. The surface potential drop behavior of the HD-SAM sample in the range of V_m = 6 - 9 V was similar to that of the ODS-SAM sample in the range of V_m = 7 - 9 V. The origin of this potential changing behavior is ascribable to the generation of polar functional groups from the methyl groups terminating the HD-SAM surface and charge trapping at oxide layers grown due to anodization of the substrate Si. At V_m = 6 and 7 V, the generation of carboxyl groups and oxidized Si was dominant,[50,51] while at V_m = 8 and 9 V the HD-SAM was considered to be removed and the remained anodic oxide layers served as charge trapping sites.

4.2.3. SCM and dC/dV-V measurement of the SAM/Si systems

As shown in Fig. 1(d) and 1(h), clear SCM images were observed in the regions where the surface potential changed, namely, the charge trapped regions as

shown in Fig. 1(c) and 1(g). The square regions scanned with V_m = 1 - 5 V on the HD-SAM sample, where there are no surface potential changes and accordingly are not modified electrically and chemically, show no SCM image changes.

After the SCM observation, dC/dV-V curves were acquired in order to elucidate the local electric properties of the patterned regions. A DC bias with the range of -4 to 4 V was applied to square-patterned regions and non-modified region for the measurements of dC/dV-V curves. Figures 3(a) and (b) show the results of the dC/dV - V measurement on the HD-SAM sample and those on the ODS-SAM sample, respectively. Minimum dC/dV-V curve peaks in corresponding unmodified regions were at -2.1 V on the HD-SAM sample and at -2.5 V on the ODS-SAM sample, respectively. The shifts of such peaks, when the ideal condition is 0 V, mean the difference of the flat band voltages. However, it is difficult to explain that such shifts are only due to the work function difference of Pt/Ir metal and Si, which is around 1.2 eV. The influence of electric dipole moment of organic molecule, negative oxide charge (native oxide layer on the ODS-SAM sample), the tip geometry, and tip-induced charge is also possibly considered as reason of negative shifts dC/dV-V curve. [28,54)]

More distinctly contrasted dC/dV-V curves acquired at un-scanned region were obtained from the HD-SAM sample than from the ODS-SAM sample. This is most likely because of the difference in total thickness of the insulating parts in the samples, i.e., 2.3 nm for the HD-SAM sample and 3.5 nm for the ODS-SAM sample.[55)] In the case of the HD-SAM sample, the peak positions and shapes of the dC/dV-V curves obtained from the regions scanned with V_m = 5 V, did not differ from a curve obtained from the un-scanned region. These results are consistent with the corresponding topographic and KFM images as shown in Fig. 1(b) and 1(c),

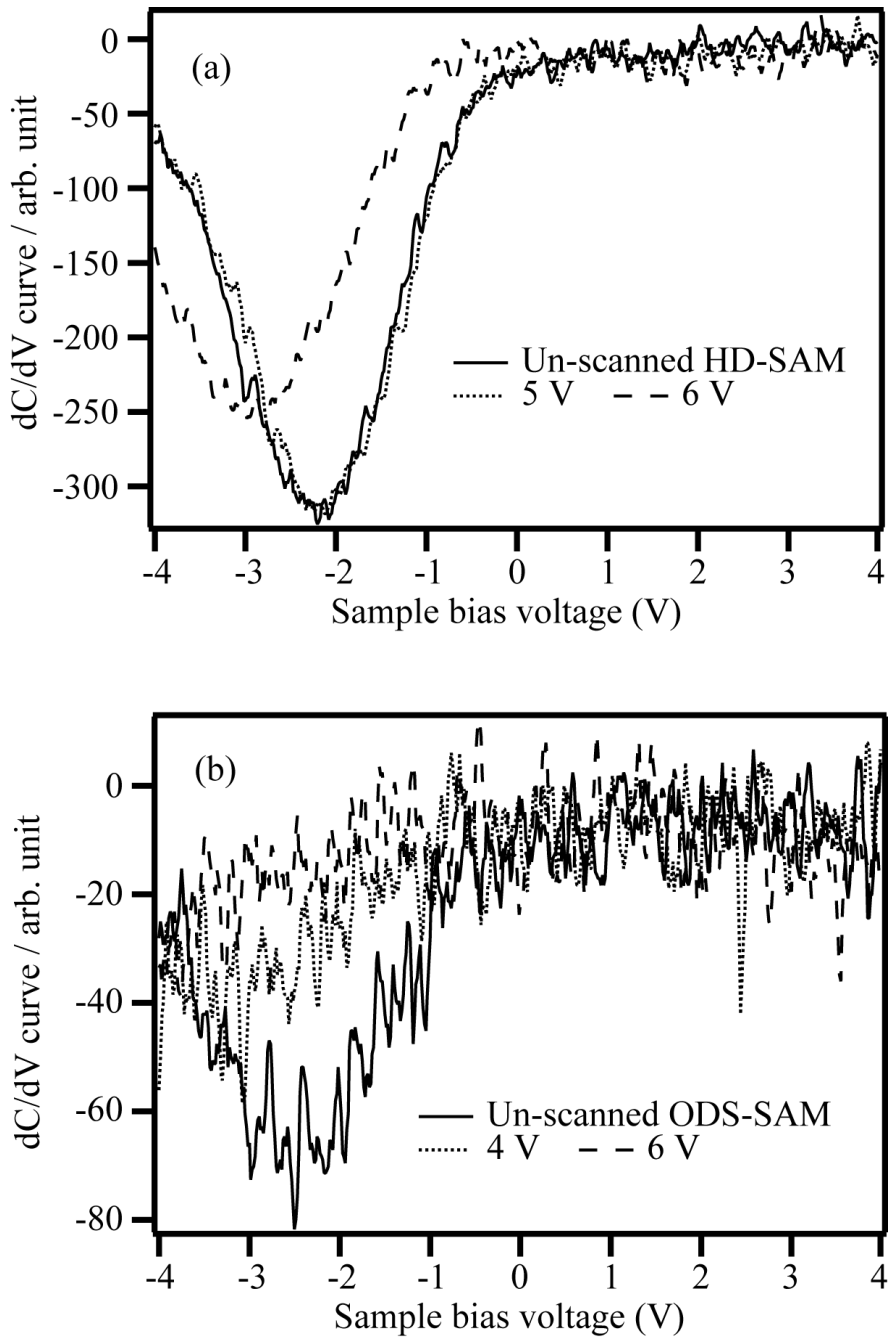

Fig. 3. dC/dV-V curves acquired from the regions un-scanned and scanned with V_m = 5, 6 V on (a) the HD-SAM sample and with V_m = 4, 6 V on (b) the ODS-SAM sample.

indicating that there is no charge trapping, chemical changes in the SAM, or anodic oxide growth. However, the peak position of dC/dV-V curve on the region fabricated at V_m = 6 V was shifted to the negative direction and the value of minimum dC/dV decreased. These are possibly due to charge trapping and change of flat band voltage by the oxidized Si.[41,47,56] In the case of the ODS-SAM sample, the width of dC/dV-V curves obtained from the regions scanned with V_m = 4 and 6 V was broadened and the position of peaks was shifted to the negative direction as compared with those of the un-scanned region. Such the widen and the shifted peaks are most certainly caused by charge traps at the Si/SiO_2 interface and SiO_2 layer, respectively.[56]

4.3. Summary

Bias effects on SAM-covered Si samples both with and without an interfacial oxide layer have been studied by using KFM and SCM. The HD-SAM system, where alkyl monolayer covalently attached to Si through Si-C bonds and formed on Si without the interfacial oxide layer, was found to have no charge trapping sites at the SAM/Si interface. On the other hand, the ODS-SAM system, in which a thin oxide layer was inserted between the SAM and Si substrate, showed distinct charge trapping behavior due to the interfacial oxide layer. We therefore expect that the SAMs directly fixed on Si are promising for very thin insulating layers with a few nm in thickness with less likelihood of charge-trap induced dielectric breakdown.

References

1) J. H. Fendler, Chem. Mater. **13** (2001) 3196.

2) R. M. McCreery, Chem. Mater. **16** (2004) 4477.

3) D. Cahen, R. Naaman, and Z. Vager, Adv. Funct. Mater. **15** (2005) 1571.

4) P. Fontaine, D. Goguenheim, D. Deresmes, D. Vuillaume, M. Garet, and F. Rondeiez, Appl. Phys. Lett. **62** (1993) 2256.

5) D. Vuillaume, C. Boulas, J. Collet, J. V. Davidovits, and F. Rondelez, Appl. Phys. Lett. **69** (1996) 1646.

6) C. Boulas, J. V. Davidovits, F. Rondelez, and D. Vuillaume, Phys Rev Lett. **76** (1996) 4797.

7) C. Zhou, M. R. Deshpande, M. A. Reed, L. Jones II, and J. M. Tour, Appl. Phys. Lett. **71** (1997) 611.

8) J. Collet and D. Vuillaume, Appl. Phys. Lett. **73** (1998) 2681.

9) S. Kar, C. Miramond, and D. Vuillaume, Appl. Phys. Lett. **78** (2001) 1288.

10) T. Graves-Abe, Z. Bao, and J. C. Sturm, Nano Lett. **4** (2004) 2489.

11) S. Maisch, F. Buckel, and F. Effenberger, J. Am. Chem. Soc. **127** (2005) 17315.

12) C. R. Kagan, A. Afzali, R. Martel, L. M. Gignac, P. M. Solomon, A. G. Schrott, and B. Ek, Nano Lett. **3** (2003) 119.

13) G. S. Tulevski, Q. Miao, M. Fukuto, R. Abram, B. Ocko, R. Pindak, M. L. Steigerwald, C. R. Kagan, and C. Nuckolls, J. Am. Chem. Soc. **126** (2004) 15048.

14) A. Krishnamoorthy, K. Chanda, S. P. Murarka, G. Ramanath, and J. R. Ryan, Appl. Phys. Lett. **78** (2001) 2467.

15) N. Mikami, N. Hata, T. Kikkawa, and H. Machid, Appl. Phys. Lett. **83** (2003) 5181.

16) J.-W. Choi and M. Fujihira, Appl. Phys. Lett. **84** (2004) 2187.

17) Q. Li, S. Surthi, G. Mathur, S. Gowda, V. Misra, T. A. Sorenson, R. C. Tenent, W. G. Kuhr, S.-I. Tamaru, J. S. Lindsey, Z. Liu, and D. F. Bocian, Appl. Phys. Lett. **83** (2003) 198.

18) Q. Li, G. Mathur, S. Gowda, S. Surthi, Q. Zhao, L. Yu, J. S. Lindsey, D. F. Bocian, and V. Misra, Adv. Mater. **16** (2004) 133.

19) N. Tajimi, H. Sano, K. Murase, K.-H. Lee, and H. Sugimura, Langmuir **34** (2007) 3193.

20) N. Saito, K. Hayashi, H. Sugimura, and O. Takai, Langmuir **19** (2003) 10632.

21) Y. Cui, Q. Wei, H. Park, and C. M. Lieber, Science **293** (2001) 1289.

22) D. Niwa, T. Homma, and T. Osaka, Jpn. J. Appl. Phys. **43** (2004) L105.

23) W. Yang and R. J. Hamers, Appl. Phys. Lett. **85** (2004) 2626.

24) S. Kobayashi, T. Nishikawa, T. Kakenobu, S. Mori, T. Shimoda, T. Mitani, H. Shimotani, N. Yoshimoto, S. Ogawa, and Y. Iwasa, Nature Mater. **2** (2004) 317.

25) K. P. Pernstich, S. Haas, D. Oberhoff, C. Goldmann, D. J. Gundlach, B. Batlogg, A. N. Rashid, and G. Schitterj, J. Appl. Phys. **96** (2004) 6431.

26) M. Halik, H. Klauk, U. Zschieschang, G. Schmid, C. Dehm, M. Schütz, S. Maisch, F. Effenberger, M. Brunnbauer, and F. Stellaccij, Nature **431** (2004) 963.

27) T. Umeda, S. Tokito, and D. Kumaki, J. Appl. Phys. **101** (2007) 054517.

28) H. Sugimura, K. Hayashi, N. Saito, N. Nakagiri, and O. Takai, Appl. Surf. Sci. **188** (2002) 403.

29) A. Hozumi, K. Ushiyama, H. Sugimura, and O. Takai, Langmuir **15** (1999) 7600.

30) H. Sugimura, A. Hozumi, T. Kameyama, and O. Takai, Surf. Interface Anal. **34** (2002) 550.

31) M. R. Linford, P. Fenter, P. M. Eisenberger, and C. E. D. Chidsey, J. Am. Chem. Soc. **117** (1995) 3145.

32) F. Effenberger, G. Goetz, B. Bidlingmaier, and M. Wezstein, Angew, Chem. Int. Ed. **37** (1998) 2462.

33) K.-A. Son, H. I. Kim, and J. E. Houston, Phys. Rev. Lett. **86** (2001) 5357.

34) D. J. Wold and C. D. Frisbie, J. Am. Chem. Soc. **123** (2001) 5549.

35) J. Zhao and K. Uosaki, J. Phys. Chem. B **108** (2004) 17129.

36) R. C. Barrett and C. F. Quate, J. Appl. Phys. **70** (1991) 2725.

37) T. Yamamoto, Y. Suzuki, M. Miyashita, H. Sugimura, and N. Nalagiri, Jpn. J. Appl. Phys. **36** (1997) 1922.

38) C. C. Williams, Annu. Rev. Mater. Sci. **29** (1999) 471.

39) M. Fujihira, Annu. Rev. Mater. Sci. **29** (1999) 353.

40) N. Nakagiri, H. Sugimura, Y. Ishida, K. Hayashi, and O. Takai, Surf. Sci. **532** (2003) 999.

41) J. Han, K.-H. Lee , S. Fujii, H. Sano, Y.-J. Kim, K. Murase, T. Ichii, and H. Sugimura, Jpn. J. Appl. Phys. **46** (2007) 5621.

42) H. Sugimura, H. Sano, K.-H. Lee, K. Murase, Jpn. J. Appl. Phys. **45** (2006) 5456.

43) H. Sugimura, Y. Ishida, K. Hayashi, and O. Takai, Appl. Phys. Lett. **80** (2002) 1459.

44) H. Sugimura, T. Hanji, K. Hayashi, and O. Takai, Ultramicroscopy **91** (2002) 221.

45) H. Sugimura and N. Nakagiri, J. Am. Chem. Soc. **119** (1997) 9226.

46) M. Yang, Z. Zheng, Y. Liu, and B. Zhang, Nanotechnology **17** (2006) 330.

47) J. W. Hong, S. M. Shin, C. J. Kang, Y. Kuk, Z. G. Khim, and S.-I. Park, Appl. Phys. Lett. **75** (1999) 1760.

48) T. P. Chen, J. Huang, M. S. Tse, S. S. Tan, and C. H. Ang, IEEE Trans. Electron Devices. **50** (2003) 1548.

49) M. L. Green, E. P. Gusev, R. Degraeve, and E. L. Garfunkel, J. Appl. Phys. **90**, (2001) 2057.

50) H. Sugimura, Jpn. J. Appl. Phys. **43** (2004) 4477.

51) R. Maoz, E. Frydman, S. R Cohen, and J. Sagiv, Adv. Mater. **12** (2000) 725.

52) J. Lu, E. Delamarche, L.Eng, R.Bennewitz, E. Meyer, and H.-J Guntherodt, Langmuir **15** (1999) 8184.

53) Y. Fukano, T. Uchihashi, T. Okusano, A. Cyayahara, Y. Sugawara, Y. Yamanishi, T. Oasa, and S. Morita, Jpn. J. Appl. Phys. **33** (1993) 379.

54) V. V. Zavyalov, J. S .McMurray, and C. C. Williams, Rev. Sci. Instrum. **70** (1999) 158

55) T. Yamamoto, Y. Suzuki, H. Sugimura, and N. Nakagiri, Jpn. J. Appl. Phys. **35** (1996) 3793.

56) S. M. Sze, Physics of Semiconductor Devices (Wiley, New York, 1981) 2nd ed., p. 375, 382, 391

5. One-dimensional arrangement of Au nanoparticles using SPA and SAM

Gold nanoparticles (AuNPs) are widely recognized as small building blocks to construct the advanced materials for electronic, optical, and sensor devices. The precise positioning and orientation of these nanoparticles on solid surfaces have received considerable attention due to their remarkable characteristics such as quantum size effect, surface plasmon resonance, and greatly enhanced surface to volume ratio.[1,2] Several methodologies have been described for the spatial arrangement of AuNPs in predefined geometries. Two- and three-dimensional assemblies of AuNPs have been investigated extensively based on self-assembly, layer-by-layer deposition, and physical vapor deposition etc.[2-5] In contrast, one-dimensional (1-D) arrays of AuNPs with precise and aligned arrangements still remain a great challenge in nanofabrication.[6] Various approaches have been proposed to construct such structures and these been categorized into two types: (a) Using linear templates such as DNA strands, nanofibres, nanotubes, nanopores, and linear polymers, but most of these approaches associated with anisotropy in particle distributions with respect to their specific scaffolds resulting in quasi one-dimensional arrangements;[7] and (b) Self-assembly/fabrication of AuNPs on predefined nanopatterns based on electron beam lithography (EBL),[8] laser patterning,[9] and scanning probe patterning etc.[10-14]

Despite the progress achieved in 1-D assembly of AuNPs, none of the aforementioned methods have demonstrated the aligned arrangement of AuNPs with controlled interpretable distances except the EBL methodology elucidated by Lennox et al.[8] This study demonstrates an elegant strategy to immobilize the AuNPs in one-dimensional arrays based on SPA[15-19] and self-assembly approaches as illustrated in Fig. 1. The SPA patterning process is versatile to construct nano-scale features under

normal conditions rather than being restricted to the harsh environments, such as high vacuum and high temperature, used in EBL.[8] Here, we employed a conformationally ordered HD-monolayer as a molecular resist film with a very smooth surface (rms roughness = 9.6×10^{-2} nm, over 1×1 μm^2). The absence of a charge trapping SiO_2 interlayer and direct covalent linkage between the HD monolayer and silicon surface provides excellent electrical characteristics.[18,20] In contrast, the alkylated/SiO_2/Si system possesses a high density of electrical active defects due to the presence of a charge trapping SiO_2 interlayer. These differences provide controlled SPA of the HD monolayer with high reproducibility.

5.1. Preparation of templates for Au nanoparticles array

The HD monolayer was prepared on a hydrogen-terminated silicon (H-Si) surface by a thermal treatment,[21] as shown in chapter 3. The water contact angle on the HD-functionalized silicon surface was found to be 109°, suggesting the formation of a conformationally ordered monolayer.[21,22] Figure 1 shows the process for 1-D arrays of AuNPs. The uniform structure of the HD monolayer was confirmed by recurrence of atomically flat terraces after formation of the monolayer (Fig. 1a). Nano-anodization of the HD monolayer was executed using the SPM with the Rh-coated silicon tip. The nanopatterning was performed using contact mode of SPM (Fig. 1b). A positive bias voltage (+10 V) was applied to the sample substrate against the tip with a scan rate of 500 nm/second. The RH of the SPM chamber was maintained as about 10% at 24 °C to reduce the water vapor concentration between the SPM-tip/HD-silicon junction. At the applied bias a localized area of the HD monolayer undergoes anodization, which leads to degradation the HD monolayer and exposes the underlying silicon surface. As a final product, the underneath silicon

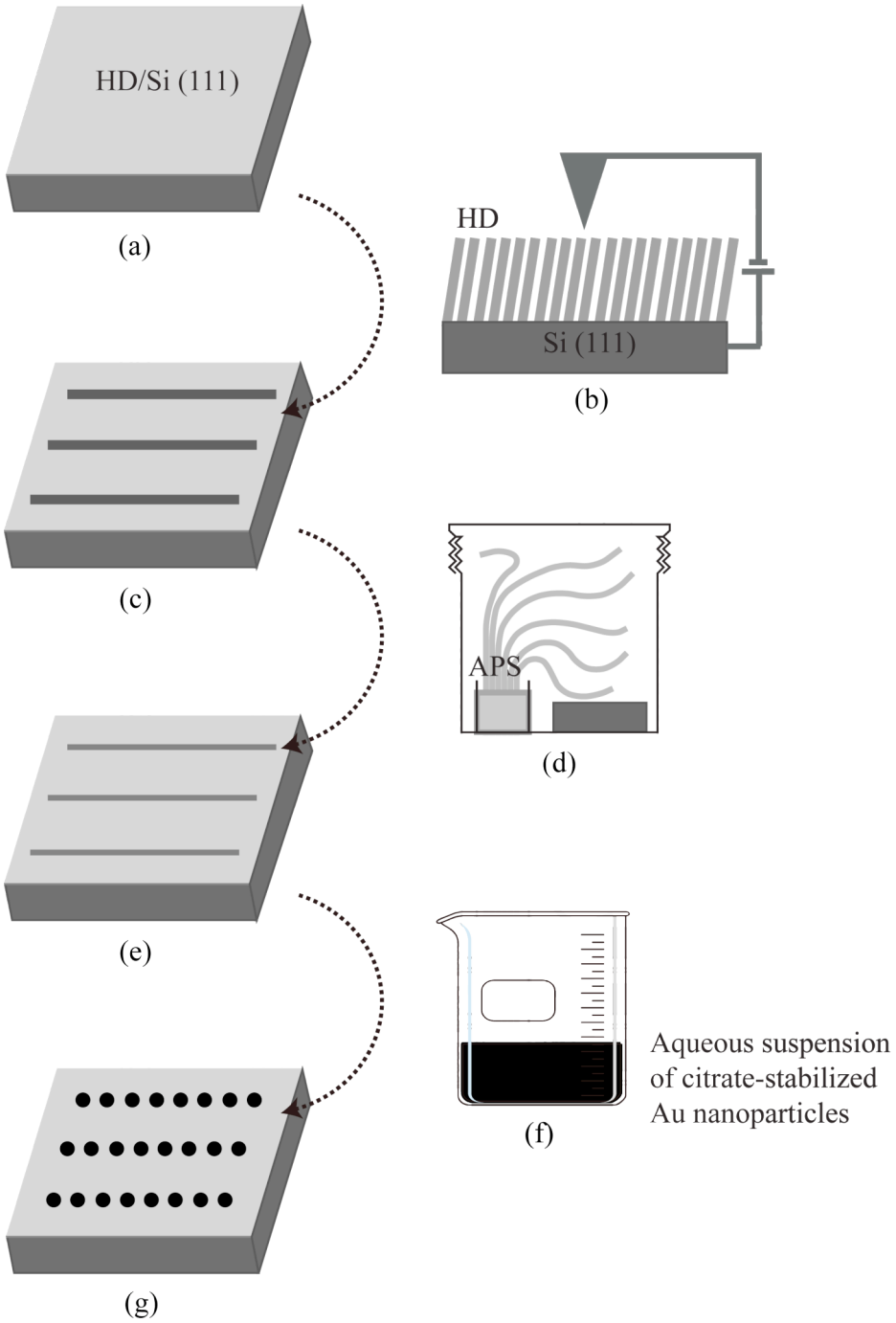

Fig. 1. Schematic illustration of (a) HD monolayer functionalized silicon sample. (b) SPA process. (c) Construction of oxidized linear features. (d) APS formation process. (e) APS monolayer functionalized linear features. (f) Anchoring process of AuNPs on the line pattern. (g) The site-selective assembly of APS monolayer guided the AuNPs immobilization.

surface was converted to a thin oxidized film (Fig. 1c). The anodized nanopattern features were constructed in a linear fashion as shown in Fig. 2. The height and a full width at half maximum of the pattern lines were found to be 1.3 ± 0.15 nm and 28.8 ± 2.5 nm, respectively. The pattern height was associated with the formation of silicon oxide due to anodization of the underlying silicon surface. The width of the pattern reduced to 14.5 ± 1 nm at the peak of the pattern line profile. Such a low pattern width was attributed to the structural order of the HD monolayer and the controlled humidity (10% RH). A 3-amino-n-propyltrimethoxysilane (APS) monolayer was deposited on pre-defined sites by a chemical vapor deposition method (Fig. 1d).[5] The strong affinity of APS towards hydroxyl/oxide moieties on pattern sites facilitated the formation of an amino terminated monolayer, while the HD covered hydrophobic surface remained untreated with the APS molecules. The quality of amino-terminated monolayer, which determines the structural organization of AuNPs, depends on the concentration of the hydroxyl groups on the patterned surface. At the reduced humidity, SPA formed oxide thin film with lack of hydroxyl moieties, resultant poor monolayer formation.[23] Recently, Liu et al. reported that the concentration of hydroxyl groups in the scanning probe oxidized SiO_2 thin film was not enough to form a good quality aminosilane monolayer.[12] In this study, before APS monolayer formation, the SPA patterned sample was treated thoroughly with ultra pure water to form a thin hydroxyl film at the pattern sites and then blown dry with stream of high purity dry nitrogen gas. The APS molecules anchored strongly to the patterned sites through Si-O-Si linkages (Fig. 1e). After APS monolayer deposition, the resulting sample was sonicated with toluene and ethanol to remove the physisorbed and/or water-mediated deposits of APS molecules on the methyl-terminated surface.[12]

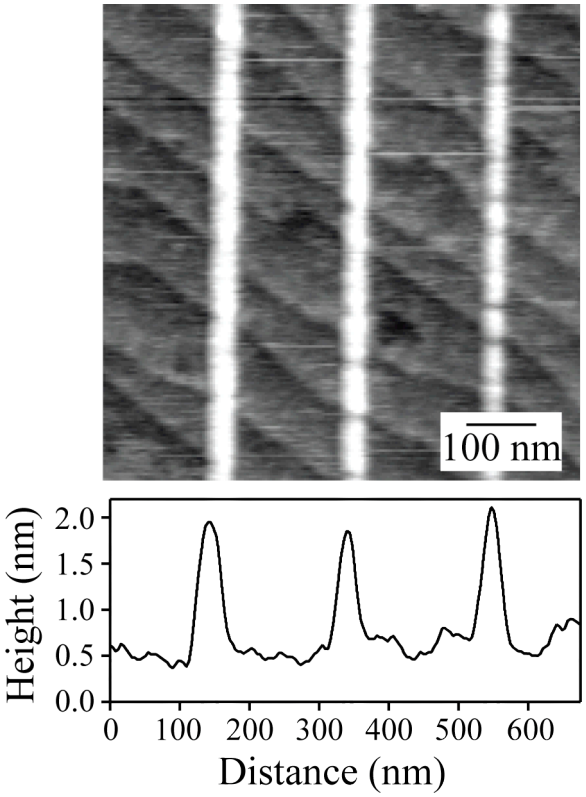

Fig. 2. Topographic image and line profile of oxidized patterns constructed on the HD functionalized silicon surface by SPA at 10% RH.

Subsequently; the chemical template was immersed into an aqueous suspension of citrate-stabilized AuNPs for one hour (Fig. 1f).

5.2. Arrangement and evaluation of Au nanoparticles

The immobilization of AuNPs on predefined sites originated from the electrostatic interaction between the citrate coating of AuNPs and the amino groups of the APS monolayer. Figure 3 shows the precise distribution of AuNPs in a linear fashion on pre-defined sites, while the HD covered surface remained unexposed to the AuNPs. The electrostatic repulsive interaction between the citrate coating of AuNPs kept them away from each other and organized them into a well-spaced orientation with a range of 12.5 to 17.2 nm as interparticle distance, revealed from Fig. 3. Note that the width of the oxidized pattern (28.8 ± 2.5 nm) constructed to direct the AuNPs was more than the particle diameter (ϕ = 20 ± 3 nm) but the electrostatic interaction forces directed the AuNPs into such a precise orientation that they were arranged into a linear fashion with a single-particle wide array. Since, the immobilization of AuNPs is directed by the self-assembly process rather than the physically monitored, hence there is minute deviation from the regular spacing between the AuNPs at few places. Such deviation occurred because of the defective nature of APS monolayer at few places due to asymmetrically distributed hydroxyl groups.[12] The close orientation between very few AuNPs, as can be seen at two-three places in Fig. 3 are probably associated to the incomplete citrate coating on AuNPs, which comes from the colloidal solution of AuNPs. These events occurred at very few places, but still most of AuNPs are regularly spaced, monitored by the electrostatic interaction. The earlier studies on two-dimensional arrangement of AuNPs on amino-terminated monolayer

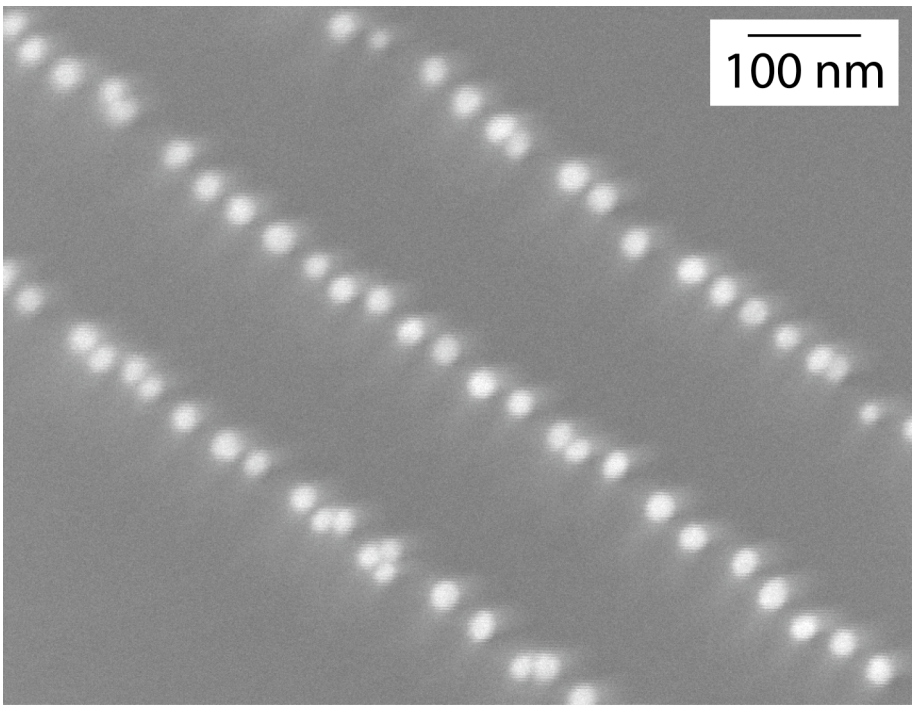

Fig. 3. FE-SEM image of one-dimensional arrays of AuNPs self-assembled on a pre-defined APS monolayer. The precise and aligned anchoring of AuNPs was determined by electrostatic interactions.

have witnessed these events by presence of di- or tri-dispersed clusters at very few places[4a, 4e, 5, 14)] due to the incomplete coating or contamination on these AuNPs.

Recently, Hartmann et al. demonstrated an Ar^+ laser-assisted procedure and formed a nanoparticle chain on a 100 nm wide strip of aminated coating where the interparticle distance was not controlled and seemed to be a quasi one-dimensional arrangement with anchoring of few nanoparticles at the non-patterned sites.[9)] There have been a few studies based on localized chemical functionalization with thiol terminal groups, which attract AuNPs and result in the formation of single-particle wide lines and wires of AuNPs, without controlled interparticle distance.[10,11)] So far, EBL has been established as a successful tool to fabricate the 1-D arrays of AuNPs with controlled interparticle distance, but the limitations arising from the complexity in e-beam exposure at the series of spots and high temperature pyrolysis, which make this approach inconvenient for exploitation at application level.[8)] The current study address the regular one-dimensional arrangement of AuNPs with monitored interparticle distance, determined by the electrostatic interaction. This approach provides a versatile means for building the 1-D architecture of AuNPs in the search for new chemically designed materials, based on single electron devices as well as development of optical wave-guides. By formation of symmetrical hydroxyl film on SiO_2 pattern and improving the quality of colloidal solution can be resolved the deviation in regular interparticle distance, and we are continuing to work on this task.

5.3. Summary

SPA of the compact HD monolayer was executed at 10% RH to construct < 30 nm wide patterns of oxidized layer. The nanopattern sites were effectively used to assemble the amino-terminated monolayer that directed the anchoring of AuNPs in a

linear fashion with an interparticle distance of 12.5 - 17.2 nm between two adjacent AuNPs. The precise and elegant strategy with preliminary results demonstrated here, promises a feasible approach to fabricate molecular electronic devices since the interparticle distance is monitored by electrostatic interactions. Changing the particle sizes and shapes as well as surrounding charge clouds could direct the magnitude of the interparticle distances resulting in alteration in the plasmonic interactions, which can be useful to develop optical wave-guides.

References

1) A. N. Shipway, E. Katz, and I. Willner, ChemPhysChem **1** (2000) 18.

2) M.-C. Daniel and D. Astruc, Chem. Rev. **104** (2004) 293.

3) G. Schmid and U. Simon, Chem. Cummun. (2005) 697.

4) (a) W. Cheng, S. Dong, and E. Wang, J. Phys. Chem. B **108** (2004) 19146. (b) A. N. Shipway, M. Lahav, and I. Willner, Adv. Mater. **12** (2000) 993. (c) S. Liu, R. Maoz, and J. Sagiv, Nano Lett. **4** (2004) 845. (d) T. Sato, D. G. Hasko, and H. Ahmed, J. Vac. Sci. Technol. B **15** (1997) 45. (e) C. -F. Chen, S. -D. Tzeng, M. -H. Lin, and S. Gwo, Langmuir **22** (2006) 7819.

5) O. P. Khatri, K. Murase, and H. Sugimura, Langmuir **24** (2008) 3787.

6) Z. Tang and N. A. Kotov, Adv. Mater. **17** (2005) 951.

7) (a) H. Nakao, H. Shiigi, Y. Yamamoto, S. Tokonami, T. Nagaoka, S. Sugiyama, and T. Ohtani, Nano Lett, **3** (2003) 1391. (b) Z. Deng, Y. Tian, S. -H. Lee, A. E. Ribbe, and C. Mao, Angew. Chem. Int. Ed. **44** (2005) 3582. (c) T. Sainsbury, T. Ikuno, D. Okawa, D. Pacile, J. M. J. Frechet, and A. Zettl, J. Phys. Chem. C **111** (2007) 12992. (d) G. -M. Kim, A. Wutzler, H. -J. Radusch, G. H. Michler, P. Simon, R. A. Sperling, and W. J. Parak, Chem. Mater. **17** (2005) 4949. (e) T. Sawitowski, Y. Miquel, A. Heilmann, and G. Schmid, Adv. Funct. Mater. **11** (2001) 435.

8) M. K. Corbierre, J. Beerens, J. Beauvais, and R. B. Lennox, Chem. Mater. **18** (2006) 2628.

9) D. Dahlhaus, S. Franzka, E. Hasselbrink, and N. Hartmann, Nano Lett. **6** (2006) 2358.

10) S. Liu, R. Maoz, G. Schmid, and J. Sagiv, Nano Lett. **2** (2002) 1055.

11) Z. M. Fresco and J. M. J. Frechet, J. Am. Chem. Soc. **127** (2005) 8302.

12) X. Ling, X. Zhu, J. Zhang, T. Zhu, M. Liu, L. Tong, and Z. Liu, J. Phys. Chem. B **109** (2005) 2657.

13) S.-D. Tzeng, K.-J. Lin, J.-C. Hu, L.-J. Chen, and S. Gwo, Adv. Mater. **18** (2006) 1147.

14) J. Zheng, Z. Zhu, H. Chen, and Z. Liu, Langmuir **16** (2000) 4409.

15) H. Sugimura, Applied Scanning Probe Methods X, Biomimetics and Industrial Applications,i (Springer, 2008), p. 217.

16) (a) H. Sugimura, T. Hanji, K. Hayashi, and O. Takai, Adv. Mater. **14** (2002) 524. (b) W. -K. Lee, S. Chen, A. Chilkoti, and S. Zauscher, Small **3** (2007) 249. (c) H. Sugimura and N. Nakagiri, J. Am. Chem. Soc. **119** (1997) 9226. (d) H. Sugimura, T. Uchida, N. Kitamura, and H. Masuhara, J. Phys. Chem. **98** (1994) 4352.

17) M. Ara, H. Graaf, and H. Tada, App. Phys. Lett. **80** (2002) 2565.

18) M. Yang, Z. Zheng, Y. Liu, and B. Zhang, J. Phys. Chem. B **110** (2006) 10365.

19) (a) J. Servat, P. Gorostiza, F. Sanz, F. Perez-Murano, N. Barniol, G. Abadal, and X. Aymerich, J. Vac. Sci. Technol. A **14** (1996) 1208. (b) R. Garcia, M. Calleja, H. Rohrer, Appl. Phys. Lett. **86** (1999) 1898. (c) R. Garcia, M. Calleja, and F. Perez-Murano, Appl. Phys. Lett. **72** (1998) 2295. (d) H. Kuramochi, K. Ando, T. Tokizaki, and H. Yokoyama, Appl. Phys. Lett. **88** (2006) 093109.

20) J. Zhao and K. Uosaki, J. Phys. Chem. B **108** (2004) 17129.

21) H. Sano, H. Maeda, S. Matsuoka, K. -H. Lee,K. Murase, and H. Sugimura, Jpn. J. Appl. Phys. **47** (2008) 5659.

22) S. Nihonyanagi, D. Miyamoto, S. Idojiri, and K. Uosaki, J. Am. Chem. Soc. **126** (2004) 7034.

23) A. Inoue, T. Ishida, N. Choi, W. Mizutani, and H. Tokumoto, Appl. Phys. Lett. **73** (1998) 1976.

6. Conclusions

This thesis has described SPA patterning of SAMs directly attached to Si substrates and evaluation of electrical properties of the structured regions on the SAM-covered Si substrates using KFM and SCM. Furthermore, for the application of the nano-structured surface, we have shown the organization of one-dimensional Au nanoparticles array.

In chapter 3, we investigated the effect of relative humidity (RH), surface hydrophilicity, and probe-tip material on features drawn during SPA. When the Rh-tip was used for SPA, the width of the anodized lines increased with increasing RH and increasing surface hydrophilicity from hydrophobic (methyl-terminated SAM surface) to hydrophilic (carboxyl-terminated SAM surface). However, under low RH of 10%, almost constant line width of about 20 nm was observed at all the SAM-covered samples. A large effect for a narrow line width, therefore, was thought to be RH rather than surface hydrophiliciy. When the CDT was used for SPA, the line width at the ester-terminated sample was a constant value of about 20 nm in spite of increasing RH. This is considered to be hydrophobic nature of the CDT, which might make a water meniscus between the tip and the sample surface narrow, and a slow hydrogen evolution rate on boron-doped diamond surface. To confirm the changes in the line width, force curves were measured. During increasing RH, the pull-off force of the CDT was almost constant, but that of the Rh-tip increased. Hence, the CDT was thought not to be sensitive to RH. We therefore think the CDT is a useful tip for SPA, due to properties independent to RH.

In chapter 4, we investigated electrical properties of the voltage-biased regions in the ODS-SAM/SiO_2/p-type Si and the ODS-SAM/SiO_2/p-type n-type Si samples using KFM and SCM. Bias voltages of 1 - 9 V were applied to each sample, with

squarely scanning tip above the sample surface. Although the surface was not modified at less than 5 V, the changes in surface potential and in differential capacitance were obtained. It was ascribed not to the degradation of the ODS-SAM but to the charge trapping and deposition in the ODS-SAM/SiO_2 interface or SiO_2 layer. The SCM particularly revealed that the charge trapping behavior was different depending on the carrier types of the Si substrates. When p-type Si was used as the substrate, the polarity of the trapped charge was inverted from negative to positive with the increase in the bias voltage for current injection, while negative charge trapping was observed for the ODS-SAM/SiO_2/n-Si all the bias range for the sample. This carrier type dependency on charge trapping could not be elucidated by the KFM observation alone. Therefore, the complimentary use of KFM and SCM is crucial for characterization of organic monolayer - semiconductor interfaces.

In chapter 5, we investigated bias effects of SAM-covered Si samples both with and without an interfacial oxide layer using KFM and SCM. The bias voltages were applied, as described in chapter 4. The HD-SAM sample without the interfacial oxide layer was found to have no charge trapping sites at the SAM/Si interface. On the other hand, the ODS-SAM sample with the interfacial oxide layer showed distinct charge trapping behavior due to the existence of the oxide layer. We therefore expect that the SAMs directly fixed on Si are promising for very thin insulating layers with a few nm in thickness with less likelihood of charge-trap induced dielectric breakdown.

In chapter 6, we fabricated the one-dimensional arrangement of Au nanoparticles using SPA method and properties of SAM terminal group. The line patterns, which were fabricated by SPA of Si substrates covered with a SAM, were effectively used to assemble an amino-terminated SAM that directed the anchoring of Au nanoparticles, due to electrostatic force between amino group and Au nanoparticle.

Such Au nanoparticles on a linear fashion were also adsorbed with an interparticle distance of 12.5 - 17.2 nm, due to negative charges existing on the Au nanoparticle surface. The precise and elegant strategy with preliminary results demonstrated here, promises a feasible approach to fabricate molecular electronic devices.

Publications

1. J. Han, K. H. Lee, S. Fujii, H. Sano, Y. J. Kim, K. Murase, T. Ichii, and H. Sugimura, "Scanning capacitance microscopy for alkylsilane monolayer covered-Si substrate patterned by scanning probe lithography", Jpn. J. Appl. Phys. **46** (2007) 5621.

2. Y. J. Kim, K. H. Lee, H. Sano, J. Han, T. Ichii, K. Murase, and H. Sugimura, "Surface chemical conversion of organosilane self-assembled monolayers with active oxygen species generated by vacuum ultraviolet irradiation of atmospheric oxygen molecules", Jpn. J.Appl. Phys. **47** (2008) 307.

3. O. P. Khatri, J. Han, T. Ichii, K. Murase, and H. Sugimura, "Self-assembly guided one-dimensional arrangement of gold nanoparticles: A facile approach", J. of Phys. Chem. C **112** (2008) 16182.

4. J. Han, D. Kasahara, T. Ichii, K. Murase, and H. Sugimura, "Scanning probe anodization patterning of Si substrates covered with a self-assembled monolayer dependent on hydrophillicity", J. Vac. Sci. Technol. B (2009) (in press).

5. J. Han, H. Sano, Y. J. Kim, T. Ichii, K. Murase, and H. Sugimura, "Charge trapping behavior of organic self-assembled monolayer/silicon systems with and without an interfacial oxide layer as studied by local current injection from an atomic force microscope tip", (submitted).

Acknowledgments

This thesis is the result of research performed at the Nanoscopic Surface Architecture (NSA) Laboratory in Kyoto University, between April 2006 and March 2009.

Firstly, I would deeply like to thank my supervisor, Hiroyuki Sugimura, for providing me with an exciting research and for financial support and his encouragement. I am also grateful to Associate Professor Kuniaki Murase for his help throughout the research. I am also grateful to Assistant Professor Takashi Ichii for many useful discussions. I am grateful to Professor Akira Sakai and Professor Hirofumi Yamada for agreeing to serve on the thesis defense committee, and for their valuable inputs to this thesis. I would deeply like to thank Professor Gil-Ho KIM (SungKyunKwan University) and Dr. Kyounghwang LEE (RIST).

The discussions that I have had with my colleagues in the NSA group were educational and are very much appreciated. I particularly must thank Dr. Yong-Jong Kim and Dr. Hikaru Sano for their help in the Ph.D course, and Mr. Jeong-Hyeon Yang for the present in the lab member.

Most important of all, I wish to thank my beloved parents, wife Yangwon Seo, for their blessings, support, and advice, which have been my motivation and guidance through every tough situation. I would like to dedicate this thesis to my children Yoobin Han and Hyunjun Han. (사랑하는 나의 아버지 나의 어머니, 감사합니다라는 말로 밖에 표현할 수가 없는 점을 용서해 주십시요. 진심으로 감사합니다. 사랑스런 아내를 주신 아버님 어머님, 진심으로 감사합니다. 나의 아내와 딸 아들, 작은 결과를 맺을 수 있었던 것은 타지에서 함께 고생해준 가족의 응원때문이였습니다. 진심으로 감사합니다.)